MIT
International Center for
Air Transportation

FLIGHT TEST REPORT OF THE JUNGLE HAWK OWL LONG-ENDURANCE UAV

Michael Burton, R. John Hansman, Tony Tao and Warren Hoburg

This report was submitted to Lincoln Laboratory MIT, Communications Systems Division in support an of a long-endurance UAV platform for communications payloads.

Report No. ICAT-2018-09
October 2018

MIT International Center for Air Transportation (ICAT)
Department of Aeronautics & Astronautics
Massachusetts Institute of Technology
Cambridge, MA 02139 USA

[Page Intentionally Left Blank]

FLIGHT TEST REPORT OF THE JUNGLE HAWK OWL LONG-ENDURANCE UAV

by

Michael Burton, R. John Hansman, Tony Tao and Warren Hoburg

ABSTRACT

Jungle Hawk Owl (JHO) is a medium altitude, long endurance, fixed wing UAV. This vehicle has been developed by MIT in collaboration with Lincoln Laboratory sponsored by the USAF Tactical Data Link and Gateways Branch, AFLCMC/HNAG at Hanscom Air Force Base. The vehicle is designed to provide long endurance (up to 5 days) communication relay for disaster relief or other communication denied environments.

The high level concept of operations includes launch from an airfield with the communications payload, flight to a disaster relief zone, loiter over the zone for at least 5 days, and flight back to the launch airfield. The requirements shown in Table 1.1 were derived from the conops. Threshold requirements describe the minimum performance criteria that the aircraft must meet. Objective requirements describe capabilities that would be desirable. Also shown in Table 1.1 are the performance capabilities of the JHO.

Specification	**Threshold (Minimum) Requirements**	**Objective (Stretch) Requirements**	**JHO Performance**
Payload	V =1 ft^3 W = 10lbs P =100Wavg	Accommodate heavier payloads without increasing vehicle size, mass and volume	V = 1.43 ft^3 W <25lbs P =100Wavg
Payload Modularity	Modular removable payload		Modular removable payload

Endurance	5 days on station	5 weeks on station	5.65 days on station
Station Keeping	24x7 coverage of fixed 100 km diameter footprint with $+5^{o}$ ground terminal elevation angle		24x7 coverage of fixed 100 km diameter footprint with $+5^{o}$ ground terminal elevation angle
Launch and Recovery	Standard Airfield	Aircraft Carrier	Standard Airfield
Latitude	$+/- 60^{o}$		Global
Availability	94%	99%	99%

Two key driving requirements are endurance and latitude. One possible architecture to meet the endurance requirement would be a solar-powered aircraft that operates on solar power during day while charging batteries and operating on battery power during the night. An initial study was done that shows that while solar-powered aircraft can achieve extended endurance, they are unable to meet the latitude requirement because of decreased solar flux and higher wind speeds at higher latitudes. Burton and Hoburg describe in detail the trade offs between gas and solar powered architectures for this kind of mission. Note that the availability was interpreted as a wind speed requirement (i.e. aircraft speed is greater than local wind speed), such that 99% availability means the vehicle can fly faster than the local wind speed 99% of the of time.

Other potential solutions to achieving aerial persistence include balloons, which can be blown off station due to winds, or through larger military drones which are cost prohibitive. The JHO offers a low cost alternative with extended endurance. The vehicle has a take off weight of 150 lbs and a projected maximum endurance of 5.6 days. It is a gasoline powered aircraft, using a 2 cylinder, 4-stroke engine. At a flight altitude of up to 15,000 ft, the JHO can provide communication coverage over a 100 km diameter footprint area.

The Jungle Hawk Owl was designed using a state-of-the-art optimization method, GPkit, that leverages convex optimization. The vehicle was optimized to maximize endurance while meeting availability, payload, and station keeping requirements. The vehicle specifications, design and performance modeling are discussed in Section 2. The designed vehicle was manufactured at MIT.

Vehicle testing and system demonstration was divided into three phases: ground testing, V0 flight tests and V1 flight tests. Ground testing involves structural load tests, engine cooling tests, and fuel flow measurements. Because the vehicle's empty or dry weight was less than 55 lbs, initial testing was accomplished under the FAA Part 107 regulation up to 55 lbs take off weight and 400 ft in altitude. This phase of testing is referred to as V0 with the objective of demonstrating launch and recovery procedures, evaluating basic handling qualities, and testing the autopilot functionality. While V0 and ground testing were ongoing, an application was submitted to the FAA for a waiver to fly at higher weights and altitudes over the Air Station Cape Cod. This second phase of testing is referred to as V1 with the objective of completing a system demonstration and evaluating vehicle performance. The results of the ground and flight tests are discussed herein.

ACKNOWLEDGEMENTS

The initial design and manufacture of the prototype were done as part of the Flight Vehicle Engineering (16.82) and Flight Vehicle Development (16.821) Department of Aeronautics and Astronautics senior capstone classes. The authors would like to acknowledge the faculty members, John Hansman, Warren Hoburg, and Mark Drela, as well as the teaching assistants and students for their enormous contribution to this project.

This work was supported by Lincoln Laboratory MIT, Communications Systems Division under a purchase agreement for the design, prototype build and prototype demonstration of the Jungle Hawk Owl.

Flight Test Report of the Jungle Hawk Owl Long-endurance UAV

Michael Burton, John Hansman, Tony Tao, Warren Hoburg

October 13, 2018

Chapter 1

Program Summary

Jungle Hawk Owl (JHO) is a medium altitude, long endurance, fixed wing UAV. This vehicle has been developed by MIT in collaboration with Lincoln Laboratory sponsored by the USAF Tactical Data Link and Gateways Branch, AFLCMC/HNAG at Hanscom Air Force Base. The vehicle is designed to provide long endurance (up to 5 days) communication relay for disaster relief or other communication denied environments.

The high level concept of operations includes launch from an airfield with the communications payload, flight to a disaster relief zone, loiter over the zone for at least 5 days, and flight back to the launch airfield. The requirements shown in Table 1.1 were derived from the conops. Threshold requirements describe the minimum performance criteria that the aircraft must meet. Objective requirements describe capabilities that would be desirable. Also shown in Table 1.1 are the performance capabilities of the JHO.

Specification	**Threshold (Minimum) Requirements**	**Objective (Stretch) Requirements**	**JHO Performance**
Payload	V =1ft^3 W = 10lbs P =100Wavg	Accommodate heavier payloads without increasing vehicle size, mass and volume	V = 1.43ft^3 W <25lbs P =100Wavg
Payload Modularity	Modular removable payload		Modular removable payload
Endurance	5 days on station	5 weeks on station	5.65 days on station
Station Keeping	24x7 coverage of fixed 100 km diameter footprint with $+5^o$ ground terminal elevation angle		24x7 coverage of fixed 100 km diameter footprint with $+5^o$ ground terminal elevation angle
Launch and Recovery	Standard Airfield	Aircraft Carrier	Standard Airfield
Latitude	+/- 60^o		Global
Availability	94%	99%	99%

Table 1.1: Design Requirements

Two key driving requirements are endurance and latitude. One possible architecture to meet the endurance requirement would be a solar-powered aircraft that operates on solar power during day while charging batteries and operating on battery power during the night. An initial study was done that shows that while solar-powered aircraft can achieve extended endurance, they are unable to meet the latitude requirement because of decreased solar flux and higher wind speeds at higher latitudes. Burton and Hoburg describe in detail the trade offs between gas and solar powered architectures for this kind of mission. Note that the availability was interpreted as a wind speed requirement (i.e. aircraft speed is greater than local wind speed),

such that 99% availability means the vehicle can fly faster than the local wind speed 99% of the of time.

Other potential solutions to achieving aerial persistence include balloons, which can be blown off station due to winds, or through larger military drones which are cost prohibitive. The JHO offers a low cost alternative with extended endurance. The vehicle has a take off weight of 150 lbs and a projected maximum endurance of 5.6 days. It is a gasoline powered aircraft, using a 2 cylinder, 4-stroke engine. At a flight altitude of up to 15,000 ft, the JHO can provide communication coverage over a 100 km diameter footprint area.

The Jungle Hawk Owl was designed using a state-of-the-art optimization method, GPkit, that leverages convex optimization. The vehicle was optimized to maximize endurance while meeting availability, payload, and station keeping requirements. The vehicle specifications, design and performance modeling are discussed in Section 2. The designed vehicle was manufactured at MIT.

Vehicle testing and system demonstration was divided into three phases: ground testing, V0 flight tests and V1 flight tests. Ground testing involves structural load tests, engine cooling tests, and fuel flow measurements. Because the vehicle's empty or dry weight was less than 55 lbs, initial testing was accomplished under the FAA Part 107 regulation up to 55 lbs take off weight and 400 ft in altitude. This phase of testing is referred to as V0 with the objective of demonstrating launch and recovery procedures, evaluating basic handling qualities, and testing the autopilot functionality. While V0 and ground testing were ongoing, an application was submitted to the FAA for a waiver to fly at higher weights and altitudes over the Air Station Cape Cod. This second phase of testing is referred to as V1 with the objective of completing a system demonstration and evaluating vehicle performance. The results of the ground and flight tests are discussed herein.

The initial design and manufacture of the prototype were done as part of the Flight Vehicle Engineering (16.82) and Flight Vehicle Development (16.821) Department of Aeronautics and Astronautics senior capstone classes. The authors would like to acknowledge the faculty members, John Hansman, Warren Hoburg, and Mark Drela, as well as the teaching assistants and students for their enormous contribution to this project.

Chapter 2

Jungle Hawk Owl Design and Manufacture

2.1 Design Overview

The JHO, dimensioned in Figure 2.1, has a pusher configuration with the engine located the in rear. A rear bulkhead acts as an engine mount and attaches to the center section of the fuselage. The center section houses two fuel tanks. The double fuel tanks, with baffles, minimizes fuel slosh while maximizing fuel volume. The front bulkhead doubles as an avionics bay and is also the primary structure for payload mounting points. The nose cone is made of Kevlar for RF transparency and houses GPS, transponder, RC, and payload antennas. A pylon attaches the wing to the fuselage and also doubles a cooling duct and air intake for the engine. The wing splits into three equal 8-ft sections. The wing has separate ailerons and flaps for redundancy in the event of a servo failure. A single-boom, conventional tail also attaches through the pylon. The tail is also made of Kevlar so that RF antennas can also be placed on the tail. The horizontal tail has two elevators for redundancy.

The DF70 engine from RCV Engines was selected as the primary engine. The DF70 is a four-stroke, two-cylinder engine that drives a 22x8 pusher propeller and is controlled by an electronic fuel injection system. An alternator is connected to the engine, and provides electricity to the avionics components and payload. A lower cost alternative engine, the TP70, was used for initial flight tests.

The aircraft utilizes an off-the-shelf autopilot, MicroPilot, for flight control. The MircoPilot was selected as a risk reduction strategy. A supervisory computer is installed to handle data flow and to issue commands to the autopilot during BLOS operations. An exploded view of the aircraft is shown in Figure 2.2 to highlight various features.

The JHO is designed to launch from a vehicle. A small skid and roller blade wheel are installed on the front and rear bulkheads for recovery. This eliminates the need for larger landing gear that adds weight and drag to the aircraft and would decrease its performance. Because the propeller radius is larger than the fuselage radius, the landing operation is done with a powered off engine.

The aircraft is designed to be as modular as possible, such that its largest dimension is only 8 ft and yet can be assembled in less than 90 minutes. It can be compactly packed into a 22x24x108 in. box, which can be shipped by Fedex. An exploded view of the aircraft is shown in Figure 2.2 to highlight various features.

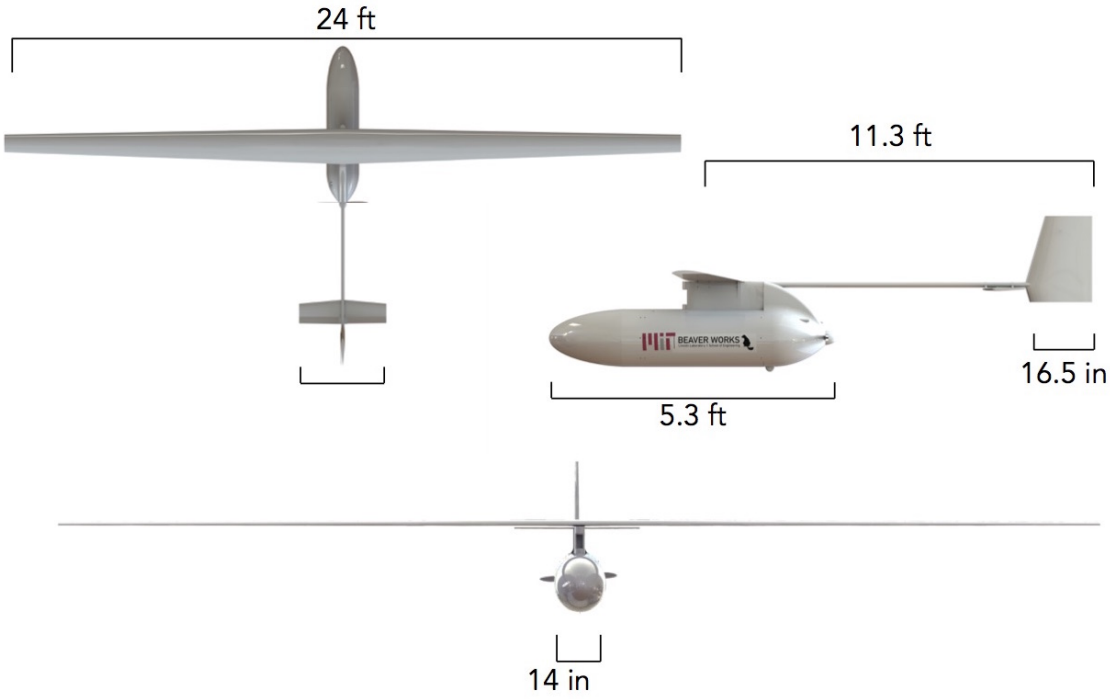

Figure 2.1: Dimensioned view of the Jungle Hawk Owl.

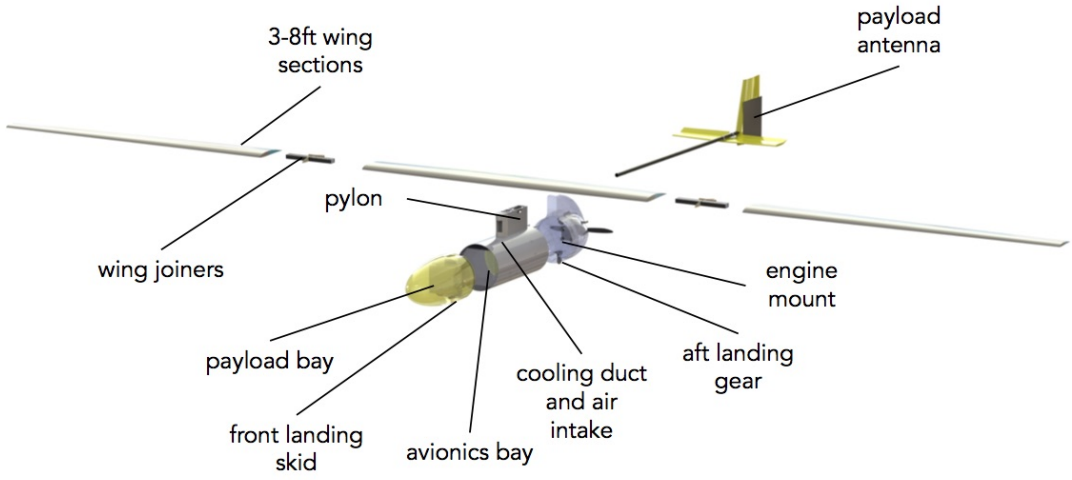

Figure 2.2: Exploded view of the Jungle Hawk Owl.

2.2 Concept of Operations

The concept of operations for the Jungle Hawk Owl includes manually controlled take off from a launch vehicle, manual to autopilot control handover, flight to coverage zone, loiter over communications coverage area, flight to recovery area, autopilot to manual control handover, manually controlled recovery operation. The con-ops is summarized in Figure 2.3.

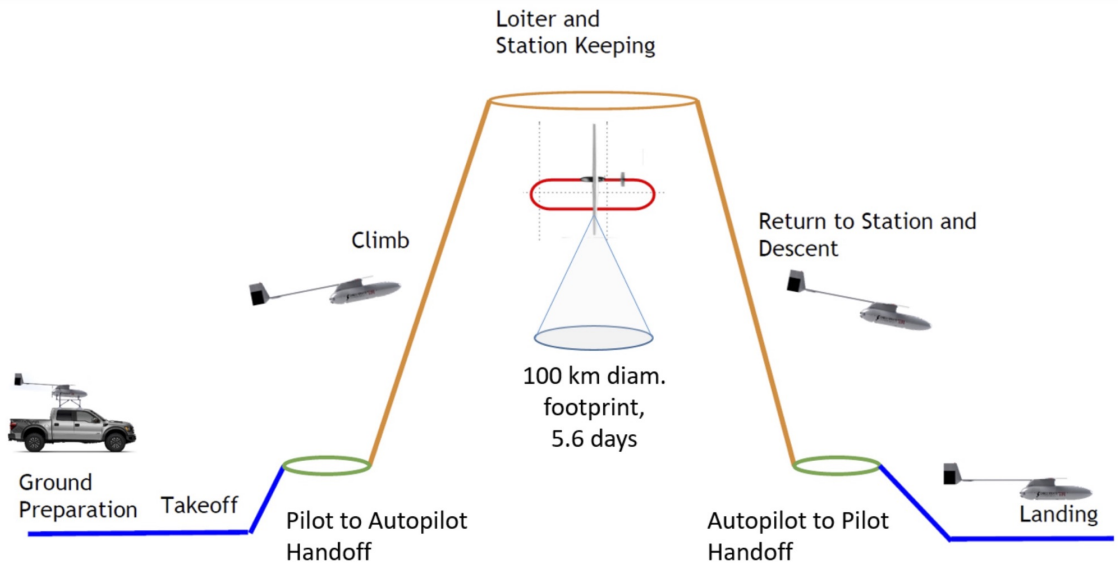

Figure 2.3: Concept of operations of the Jungle Hawk Owl.

Takeoff is performed within visual range of a ground-based pilot who has direct control of the aircraft through a UHF controller included with the ground station. The aircraft is held to the launch rack by a positive release mechanism controlled by a UHF controller. The launch vehicle, driven by an operator, accelerates to the aircraft's rotation speed. When rotation speed is reached, the pilot releases the aircraft from the launch rack and performs a pull-up maneuver to allow the aircraft to separate from the vehicle. The aircraft launch requires less than 1050 ft of straight road (paved or unpaved) for takeoff, considering the acceleration and braking distance of typical vehicles.

After takeoff, the ground-based pilot transfers control authority of the aircraft to the autopilot system. The aircraft autonomously climbs to the loiter altitude of 15,000 ft. The aircraft then cruises to the communication support zone. Upon arrival, the aircraft follows waypoint-based commands to autonomously loiter for the required mission duration. The aircraft's payload provides a communication link between ground units that are beyond line-of-sight (BLOS) from each other. Communication between the aircraft and its operators is maintained through a satellite-based Internet system, which allows operators to receive telemetry data regarding the aircraft's systems.

When the mission is complete, the aircraft autonomously cruises back to its landing location, and the ground-based pilot manually lands the aircraft within line of sight using the UHF radio. After landing, the ground team performs the necessary maintenance. The aircraft is able to launch within 6 hours if more communication coverage is required. Multiple aircraft can be coordinated to provide extended persistent coverage or cover adjacent sectors.

2.3 Vehicle Design and Performance Estimates Using GPkit

There were important, multidisciplinary trade-offs that needed to be understood in order to optimize the size of the Jungle Hawk Owl. To correctly understand these trade-offs GPkit was used. GPkit is a convex optimization framework being developed at MIT, that leverages geometric programming optimization. This optimization framework allowed for the synergistic design of all subsystems of the aircraft. Each subsystem (aerodynamics, structures, propulsion, avionics, operations) is modeled by governing equations specific to their discipline and combined into a comprehensive optimization model.

GPkit was used to both size the aircraft and predict performance. Table 2.1 shows overall aircraft dimensions and performance that were calculated using GPkit and used in the actual design. Both the maximum endurance of the aircraft and the endurance with the required payload and availibility are shown.

The optimal endurance speed of the aircraft varies depending on the weight. To maximize endurance

Specification	Value
Dry Weight (with 10 lb payload)	55 lbs
Take off Weight	143 lbs
Maximum Endurance	6.77 days
Endurance with 10 lb payload and 95% availibility	5.56 days
Maximum speed	105 knots
Maximum payload capacity	20 lbs
Maximum payload power draw	200 W

Table 2.1: JHO performance specifications.

the aircraft will fill at the optimum endurance speed, which will decrease as fuel is burned the weight of the aircraft decreases throughout the flight. The optimum speeds and weight change for the JHO, calculated using GPkit, over its maximum endurance time of 6.77 days are shown in Figure 2.4. If the aircraft is flying in wind speeds that are faster than the optimum endurance speed the vehicle will fly directly into the wind maintaining zero ground speed. If the wind conditions are slower than the optimum endurance speed the vehicle will fly a holding pattern over the desired area.

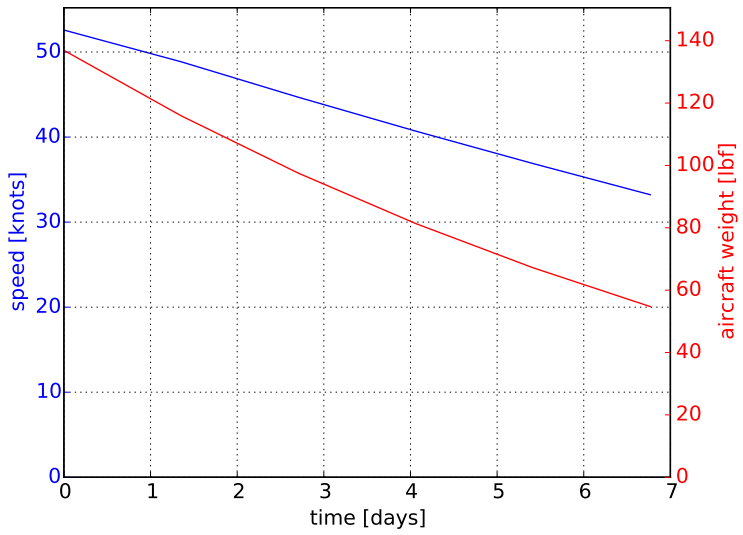

Figure 2.4: Speed and weight change during maximum endurance mission for JHO.

If the JHO is constrained to fly a constant speed for the duration of the mission, its endurance must be less than 6.77 days. Slower speeds will result in high lift and high drag limiting the endurance of the aircraft. Faster speeds will result in high fuel consumption also limiting the endurance. The trade off between constant aircraft speed and endurance is shown in Figure 2.5. Also shown in Figure 2.5 is the maximum endurance of the JHO if the speed is allowed to vary during the mission.

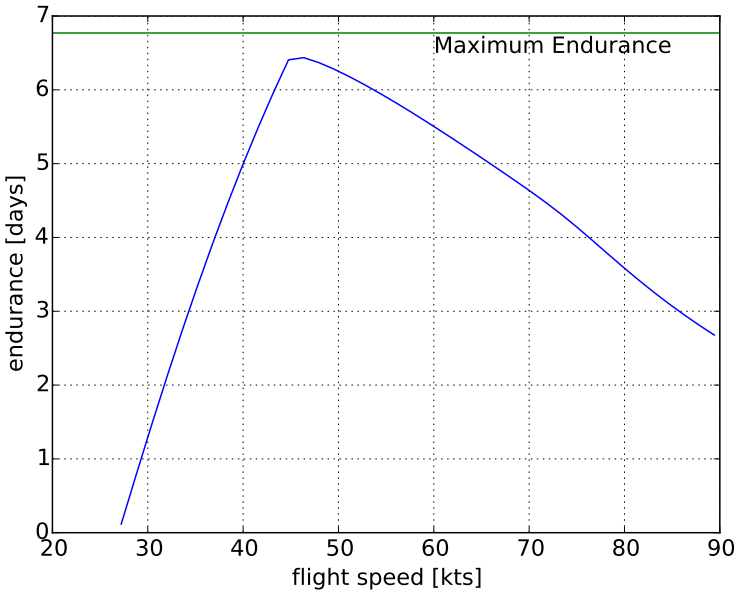

Figure 2.5: Endurance performance estimates at different constant loiter speeds. Maximum endurance allows variable loiter speed.

The JHO can support payloads up to 20 lbs. The design payload weight is 10 lbs, meaning that payloads that weigh more than 10 lbs will reduce the endurance and payloads less than 10 lbs will increase the endurance. Figure 2.6(a) shows the trade off between payload weight and endurance.

The payload weight of the aircraft is limited by its longitudinal stability. The aircraft is designed to have a stability margin of 5% with a 10 lb payload, which presents a good compromise between static stability and low trim drag during loiter. The aircraft is able to accommodate higher payloads with the same static margin by allowing for the addition of lead ballast in the tail boom, which offsets the forward CG shift because of changes in payload mass. This allows the longitudinal control characteristics of the aircraft to stay similar regardless of the payload size. Because the structural margin of the aircraft decreases as the payload weight increases, it is recommended that the payload weight of the aircraft does not exceed 20 lbs.

There is also a trade off with endurance if additional power is consumed by the payload during flight. This trade off is shown in Figure 2.6(b). Because the aircraft avionics systems draw 65 W and the alternator capacity is 200 W, the payload power is limited to 135 W. Power requirements greater than 135 W may require a new alternator or new combination of engine and alternator.

	Top of Climb	Cruise	Loiter Start	Loiter End
Altitude [ft]	0 - 15000	15000	15000	15000
Total Power Requirement [hp]	2.47	1.46	1.14	0.69
Equivalent Sea Level Power [hp]	5.12	2.98	2.35	1.43
Engine RPM	7750	6800	6400	5800

Table 2.2: Engine power requirements during flight

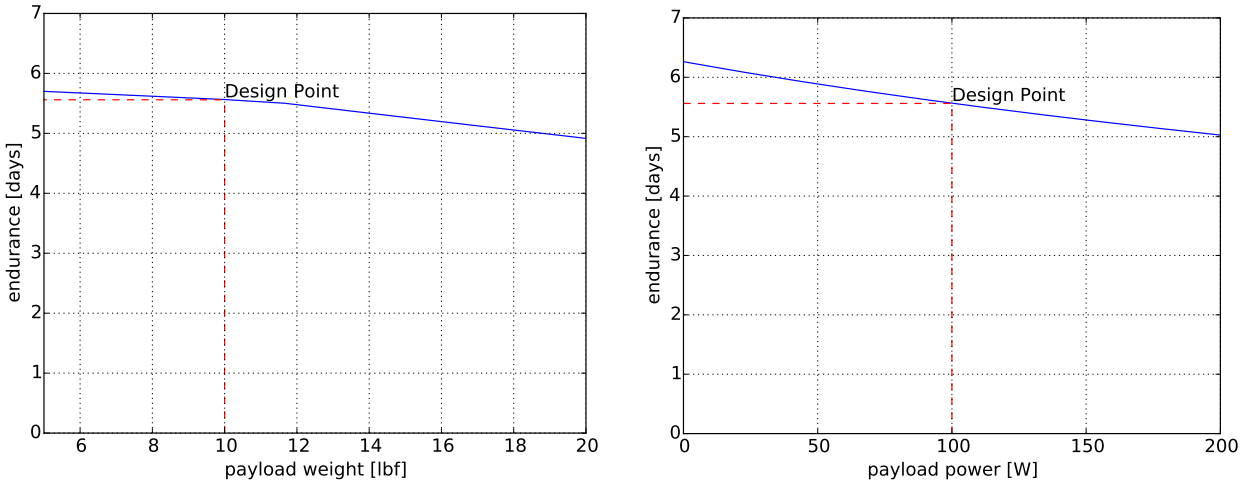

(a) Endurance vs payload weight

(b) Endurance vs payload power

Figure 2.6: Endurance trade studies for different payload weight and power requirements.

2.4 Propulsion

The propulsion system was designed to meet the following requirements:

- Provide sufficient propulsive power during all stages of flight as shown in Table 2.2
- Provide 100 W of continuous electrical power to the payload, 130 W to the avionics system and 30 W to the Electronic Fuel Injection (EFI) system during a surge (total 260 W)
- Achieve a brake specific fuel consumption (BSFC) of at least 0.57 lb/hp/hr during cruise.

The DF70 engine was selected from RCV Engines because it met the propulsion requirements and because of its reliability. The DF70 is a two cylinder, four-stroke cylinder. The engine and basic specifications are shown in Figure 2.7 and Table 2.3.

The DF70 engine comes with a pre-installed fuel injection system and alternator. The high cost is due to the high efficiency of the engine and the reliability of the entire system as a whole. The recommended alternator for this engine is the Sullivan S676-300F alternator (Figure 2.8). It can supply up to 475 W at 7500 RPM and 120 W at 2500 RPM. By extrapolation, the alternator can supply about 350 W at 5800 RPM at the end of the loiter phase. Thus, at the lowest expected RPM during flight, the alternator meets the minimum 260 W requirement to power the aircraft avionics and payload system.

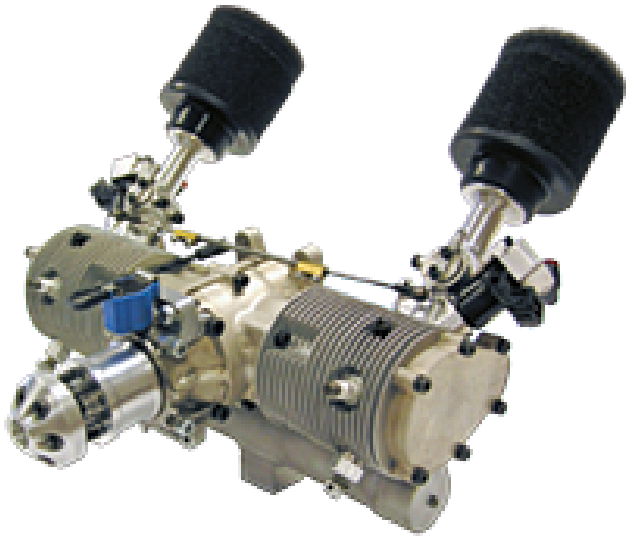

Figure 2.7: DF70 Engine from RCV Engines, Ltd.

Specification	Value
Capacity	70 cc
Max Power	5.4 hp
Speed range	2000-10000 rpm
Average BSFC	0.54 lb/(hp.hr)
Weight	5.9 lb
TBO	500 hrs
Cost	$\sim$ \$20000

Table 2.3: DF70 Specifications.

Figure 2.8: Sullivan S676-300F alternator for DF70 engine.

A low cost alternative to the DF70, the TP70 (Figure 2.9 and Table 2.4), was explored and used on initial tests. While the BSFC was not specified by the manufacturer, initial ground tests showed that BSFC of the TP70 was similar to that of the DF70. One disadvantage of the TP70 is that it does not come pre-installed fuel-injection system or alternator. Significant modification was required to install and test these components. Initial flight tests revealed several reliability issues with the TP70, which are explained in Chapter 4.

2.4.1 Engine Cooling

The cooling duct is sized to meet the cooling requirements at take-off, with considerations taken in the design to reduce the cooling drag. The duct intake is 6.2 in^2, and is situated in the wing pylon. This sizing allows for sufficient cooling flow, and allows for the inlet-to-outlet area ratio to be approximately 2-4, which is typical for many vehicles. This ratio allows sufficient flow acceleration to avoid flow reversal without drastic speed increases in the flow. The inlet is situated in the middle of the pylon so that the duct does not ingest air from the boundary layer on the fuselage of the aircraft. The cooling inlet also doubles as the engine air intake.

Air flow simulation was done in SolidWorks to verify that the engine cylinder head temperatures would not exceed 160^o C, or the do-not-exceed limit prescribed by the manufacturer. The study was done to simulate cooling at maximum power draw during take off and climb. Air velocity, air density, and engine

Figure 2.9: TP70 engine from TorquePro.

Specification	Value
Capacity	70 cc
Max Power	6.2 hp
Speed range	2000-10000 rpm
Weight	4.4 lb
Cost	∼ $700

Table 2.4: TP70 Specifications.

power were set as flow parameters in the simulation. The maximum simulated temperature was 145^o C. Ground and flight tests were done to validate this result.

2.5 Avionics

The two primary communication links to the Jungle Hawk Owl are through the autopilot and RC control. The MicroPilot autopilot was used as an off-the-shelf risk reduction component for autonomous command and control. The RC communication is done through off-the-shelf Spektrum transmitters and receivers also at 2.4 GHz. For LOS operations the autopilot communicates to the ground control station through a 2.4 GHz radio link. For BLOS operations a secondary computer receives commands from the ground station through the iridium network and relays them to the autopilot. The aircraft is also equipped with a transponder. A summary of the command and control communications components is shown in Table 2.5.

Control Type	Make/Model/ Manufacturer	Frequency	Link Range	Power Source
RC Control	Spektrum RC DX18 transmitter AR9110 receiver	2.4 GHz	∼1 mile	Rechargeable 6 cell LiPo battery pack
MicroPilot GCS Radio Link	MHX2420 Microhard	2.4 GHz	30+ miles	External power source
Iridium Satellite Modem	RockBlock MK2	1610-1626.5 MHz		UAS onboard power
FTS Control	Spektrum DSMX (directional antenna)	2.4 GHz	∼10 miles	Independent 4S NiMH battery
Navigation/GPS	Ublox AMY-6M 5Hz receiver	1575.42 MHz		UAS onboard power
Transponders	uAvionix Ping20Si	1090 MHz		UAS onboard power

Table 2.5: Command and control components

The MP2128 MicroPilot is an off-the-shelf autopilot and was selected in lieu of a custom made or open source autopilot to minimize system risk. It communicates to the ground station through Microhard MHX2420 antennas with 30 mile link range. The MicroPilot allows for in-flight waypoint adjustments. It also contains pre-programmed failure modes for risk mitigation. While initially attractive, the MicroPilot has several downsides. Because the servo control board is directly linked to the MicroPilot, the servo and RC receiver power are linked to the MicroPilot eliminating the use of RC backup control in the event of a MicroPilot power failure. Additionally, because the software is proprietary, customized changes for failure modes and flight test plans are not possible.

RC control is done through the DX18 Spektrum transmitters and receivers. Multiple receivers are placed in the nose cone and vertical tail of the aircraft for redundancy. Each receiver is paired to a specific transmitter which is encrypted. The unique pairing of transmitter and receiver prevents any hostile RC takeover. However, the unique pairing also prevents RC control hand-off to a separate receiver. Operationally, this restricts the launch and recovery to occur at the same location and prevent RC backup control during an emergency situation if the aircraft is out of range of the transmitter.

During BLOS operations commands are passed from the ground control station through the iridium network to the secondary computer onboard the aircraft. The aircraft is equipped with an iridium antenna that operates at 1610 MHz. The secondary computer then relays the command to the MicroPilot. A RaspberryPi was selected as the secondary computer because of its size, cost and modularity. The RaspberryPi is also used to read values from the engine ECU and fuel flow sensor including RPM, fuel pressure, cylinder head temperatures and fuel flow rates. These parameters are transmitted to the MicroPilot and read on the ground control station through the 2.4GHz MicroPilot radio link.

A flight termination system, explained in Section 2.7, is controlled using a Spektrum transmitter with a custom installed directional antenna. It is independent of the RC and MicroPilot control links.

The avionics are powered through the alternator during flight. The power is routed through a power management unit, which powers a 24V and a 5V line. When the engine is not running during start up and post-recovery, the avionics are powered off of a 6S LiPo battery. The battery is charged by the alternator during flight and provides up to 1 hour of power for emergency maneuvers in the event of an engine-out failure.

2.6 Launch and Recovery System

The takeoff mount is composed of an off-the-shelf Yakima Baseline roof rack, aluminum tubing, and steel connectors. The aircraft is held in a rear cradle slightly behind its CG. This launch rack has been installed on multiple vehicles including a Mazda, Ford F250, Ford Explorer and Ford Ranger. The front cradle holds the aircraft at a nose down incidence angle during acceleration. A solenoid-actuated retention pin keeps the aircraft on the rack until release. During launch, this pin is disengaged by a pilot or other ground crew operator via an RC controller.

(a) Solenoid-actuated retention pin

(b) Side view of JHO in launch rack

Figure 2.10: Launch mechanism and rack.

The propeller is mounted such that it will stop in a horizontal position in most cases to avoid propeller strike during landing. In the event the propeller stops in the vertical position, it is frangible and will break on touchdown. There is no restart capability on this aircraft, so once the engine is cut, the pilot is committed to landing the aircraft. Normal touchdown is at a positive pitch angle to create contact with the back landing wheel. The aircraft will pitch forward onto the front landing skid and then come to a stop.

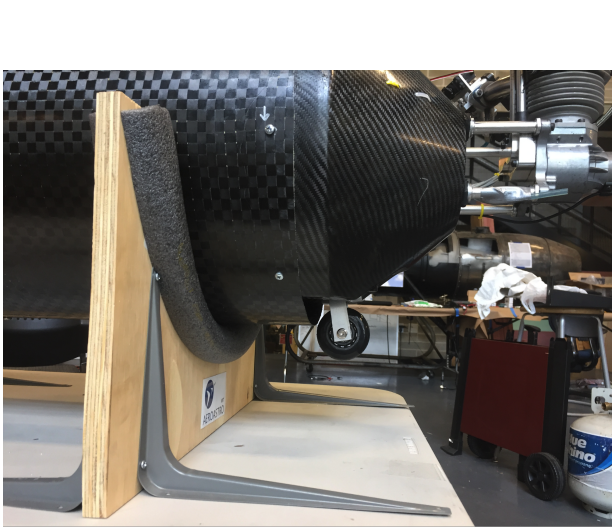

(a) Landing gear placement on rear bulkhead

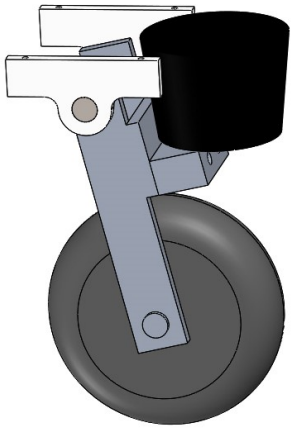

(b) Landing gear design

Figure 2.11: Landing gear design and placement

For initial flight testing, a launch protocol was created to minimize risk to the aircraft and ground crew. When the driver is lined up with the runway, the driver will communicate with the pilot and GSC to confirm takeoff roll. Once confirmation is received, the driver speeds up to the launch reference speed. Once at the reference speed, the driver relays his speed to the pilot. When the pilot is ready, he commands the release to unlatch the aircraft for take off. At separation, the driver shall pull to the downwind side of the runway and decelerate. If there is a malfunction, the driver will begin to slow down after crossing a designated "abort point" on the runway

2.7 Flight Termination System

The flight termination system (FTS) is designed to end the flight of the Jungle Hawk Owl (JHO) UAV and was implemented for flight testing as a risk reduction measure against departure of the vehicle from designated airspace. The design prioritizes containment distance over vehicle survivability. The FTS overpowers both manual and autopilot controls and makes level flight impossible sending the aircraft into a controlled downward spiral by means of a wing tip parachute.

2.7.1 Design

The FTS is composed of a servo-released parachute that is mounted on the wingtip of JHO. The FTS deployment cannot be triggered by the autopilot, satellite datalink, or primary flight transmitter. Once deployed, the FTS cannot be disengaged. A photo of the installed FTS system is shown in Figure 2.12

Figure 2.12: Installed flight termination system on left wing.

A dedicated FTS radio transmitter equipped with a directional antenna operates from the ground. An on-board receiver commands the actuation of the deployment servo. The radio system has a link range of 10 miles and is encrypted such that no external interference can accidentally trigger the deployment of the FTS. For future versions of the JHO it is recommended that the FTS system be linked the RaspberryPi such that it could be deployed during operations beyond 10 miles from the ground station. Power for the FTS is provided by a dedicated 4s NiMH battery that is trickle-charged by the aircraft's power bus. A diode prevents back-feed from the FTS to the vehicle power bus. This ensures that the FTS will have sufficient power to operate regardless of the mission duration, and will still be active in case of power system failure on JHO. The battery provides at least 1 hour of standby power after the removal of the servo bus power.

2.7.2 Operation

The parachute produces a large sustained drag force to the wingtip, preventing uncontrolled downrange or out of range flight. There are two primary phases of operation for the parachute. These modes will be designated as the "yaw phase" and the "spin phase". The yaw phase occurs just after deployment when the vehicle is still flying level. The yaw torque generated by the parachute is far greater than the yaw torque generated by the vertical tail (even with the rudder deflected against the direction of yaw).

The yaw load causes the aircraft to enter a substantial sideslip, decelerating the left wing and accelerating the right wing. The reduced effective span and side-slipped configuration causes the aircraft to descend and start the spin phase.

During the spin phase, the vehicle descends quickly and the parachute maintains a drag force that pulls the left wingtip skywards. During this phase, tight spins to both the right and the left are possible. If throttle is low, the small angle of attack of the incoming airspeed against the wing produces a right-turn force that generates a continuous turn to the right. If throttle is high and the ailerons are configured to roll-left, the aircraft may flatten its spin at which point the increased velocity on the downward wing is able to generate a left-spin. If the forces are in perfect balance, a knife-edge descent may be possible, though this mode is unlikely. Diagrams describing both the forces and resultant behavior of the aircraft if the FTS is deployed are shown in Figure 2.13

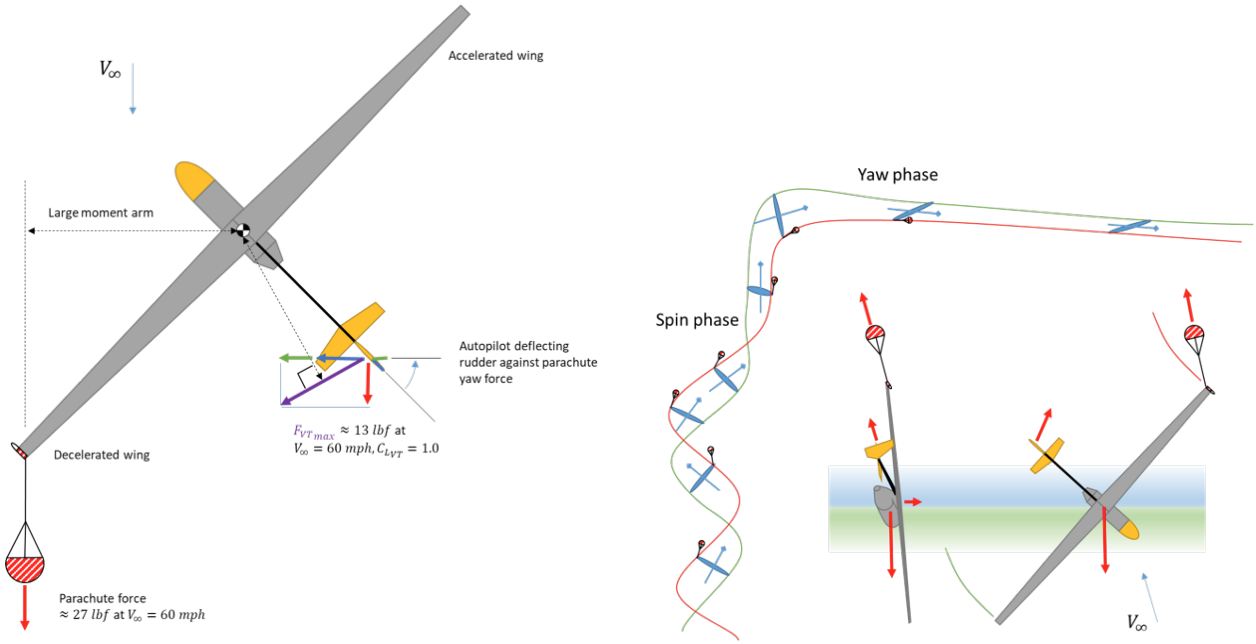

(a) Forces during parachute-induced spin entry

(b) FTS descent concept showing right-hand spin (most common)

Figure 2.13: FTS forces and descent concept.

2.7.3 Simulation

A simulation was conducted in X-Plane 11 to predict the behavior of the vehicle once the FTS is deployed. Altitude was set at 10,000 ft and VTAS was 54 knots at FTS deployment. The airport shown in the maps is Plum Island (2B2) to provide sense of scale. During this simulation, a conventional autopilot was activated (with default settings) to simulate the autopilot resisting the effects of the FTS. The figure below shows the autopilot applying opposite-rudder to resist the yaw torque from the parachute. However, the parachute overpowers the rudder and enters the aircraft into a spin.

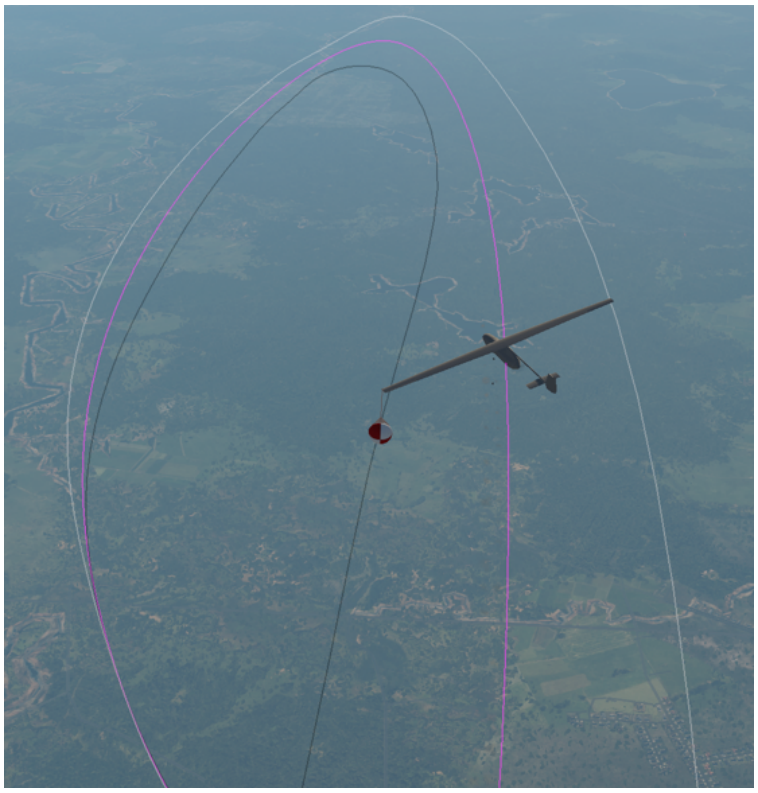

Figure 2.14: FTS deployment and flight track.

The descent is dominated by the right-spin mode. During descent, the VTAS was predicted to be approximately 60 knots. The descent from 10,000 ft took 126 seconds and ground contact occurred 1750 ft from the location at which the FTS was activated. A downrange excursion distance of 0.20 ft per 1 foot of altitude is expected.

2.8 Prototype Manufacture

An initial prototype of the Jungle Hawk Owl was manufactured at MIT. The fuselage, fairings, wings and tail are composite materials manufactured using one-sided molds and a vacuum bagging curing process. The dimensions of each component were determined using the GPkit optimization model. Detailed design was done at the component level. The estimated weights of each component from the GPkit model are compared to the actual manufactured weights in Figure 2.15.

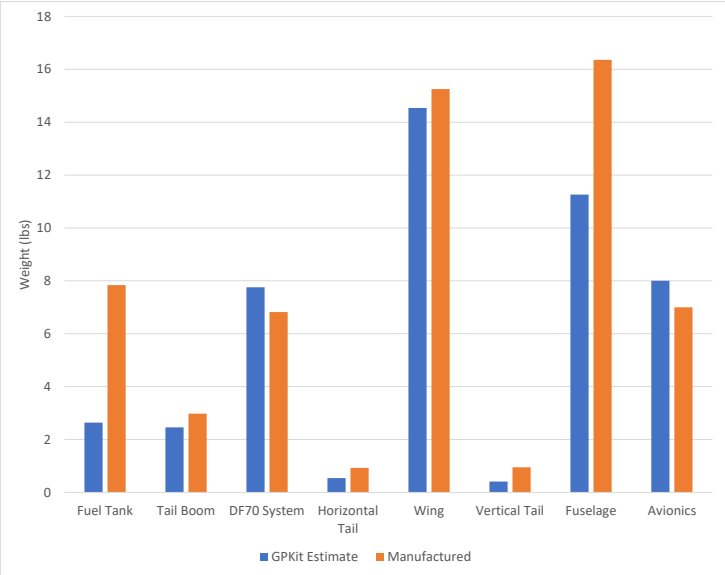

Figure 2.15: Weight comparison of estimated GPkit weights and manufactured weights.

Figure 2.15 shows that the wing, horizontal and vertical tail weights were well approximated by the GPkit model. The most notable differences are the fuel tank and fuselage. The design fuel tank is a custom made polymer material designed to maximize fuel volume. To avoid program costs and delays, an initial fuel tank was manufactured out of aluminum for flight testing accouting for the weight discrepency between the GPkit estimate and manufactured weight. The discrepancy in the fuselage weights occurred because it was decided to increase the strength of the fuselage structural components by adding material after initial component prototypes were manufactured.

2.8.1 Wing

The 24 ft span wing was manufactured in three equal 8 ft sections. The primary structure of the wing is spar, which consists of two unidirectional carbon fiber caps separated by a foam core and wrapped in a carbon fiber shear web. Two wing joiners were manufactured to connect the inboard and outboard sections. The wing joiners were designed and manufactured in a similar way to the wing spar to help transfer the load from the outboard sections to the center section. Two aluminum plates attach to the spar at the center of wing and act as mounting points to the fuselage.

The aileron and flap servos are mounted on 3D-printed parts, which are embedded inside the wing. The top surface of the wing surface was painted white for heat protection and visual observance during flight. Images of the wing installed on the aircraft are shown in Figure 2.16.

(a) Center wing section post-curing

(b) Installed wing on aircraft

Figure 2.16: Wing shown post-curing and installed on aircraft.

2.8.2 Fuselage

The fuselage main structural elements consists of the carbon fiber center section, the pylon, and front and rear bulkheads. The pylon, which has aluminum inserts for hard mounting points, is wrapped in carbon fiber and serves as wing mount, tail boom mount and engine cooling duct. The center section is 14" in diameter and has a carbon fiber, Kevlar, carbon fiber structure for added strength. It attaches to the pylon through two longerons. The rear bulkhead is conical in shape and also has a carbon fiber, Kevlar, carbon fiber structure. The shape gives it added strength to mount the engine and allows for increased fuel volume. The front bulkhead is made of carbon fiber and also acts as the avionics bay. A lid on the avionics bay is also made of carbon fiber and has hard mounting points for the payload.

The front and rear fairings were made with one sided molds. The front fairing was made of Kevlar for RF transparency. Vents were installed on the rear fairing for engine cooling exhaust. The pylon fairing was made out of plastic using thermal forming on a male mold. A labeled view of the fuselage as well as the constructed fuselage is shown in Figure 2.17.

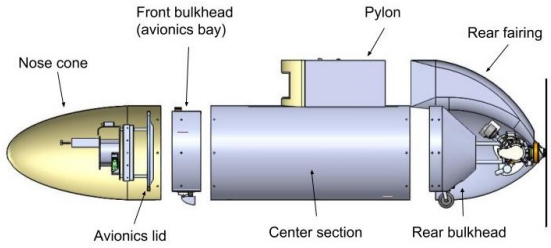

(a) Exploded fuselage view

(b) Manufactured fuselage

Figure 2.17: Diagramed and manufactured fuselage.

The avionics bay holds all primary electronics systems including the battery, PMU, MicroPilot, RaspberryPi, servo control chips and supporting electronics. The avionics bay is shown in Figure 2.18.

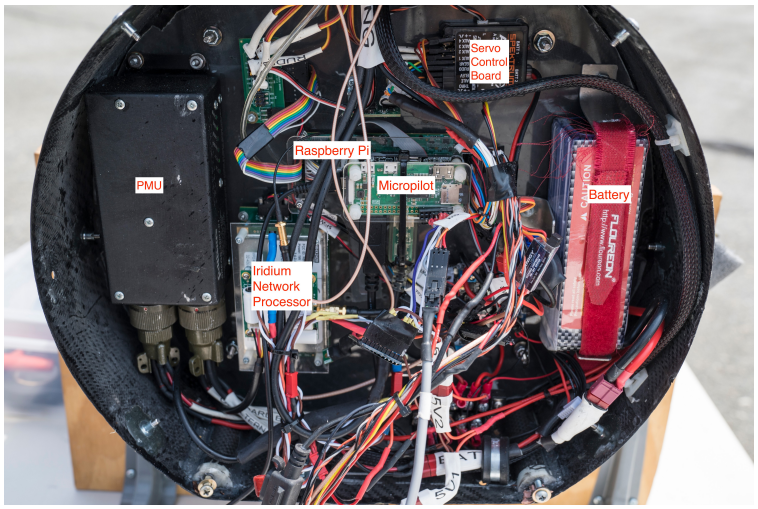

Figure 2.18: Manufactured avionics bay.

2.8.3 Empennage

The tail is composed of a horizontal stabilizer and a vertical stabilizer and tailboom. The horizontal section is symmetric about the boom, and vertical tail is located aft of the horizontal piece. The horizontal tail is secured beneath the boom and has two separately controlled elevators located at 30% of the root chord on the horizontal tail. The vertical tail contains a single rudder similarly located at 30% of the root chord. The vertical tail contains an externally-mounted payload patch antenna. All tail pieces are cut from Highload 60 foam and wrapped in 0.01" of Kevlar for structural stability and for RF transparency. Both the vertical and horizontal sections are NACA 0008 airfoils. Carbon fiber brackets attach the tail boom to the vertical and horizontal tails. Figure 2.19 shows the completed empennage.

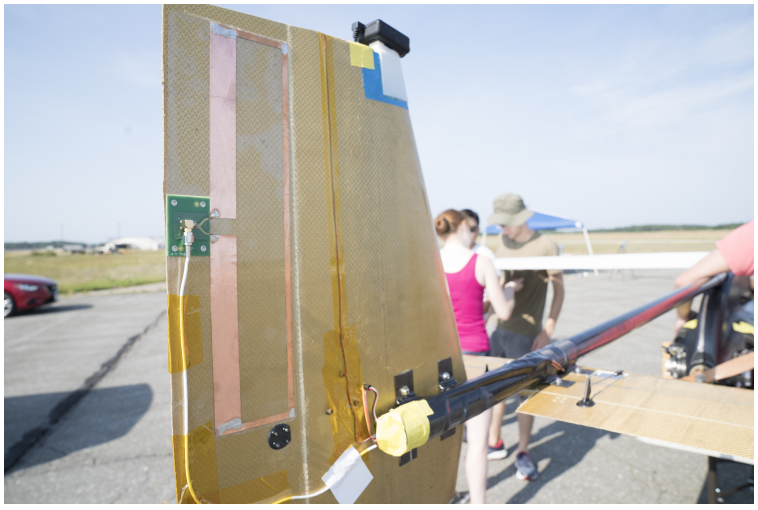

Figure 2.19: Manufactured empennage.

2.9 Vehicle Cost Estimation

It is estimated that the at-scale, unit production cost of the Jungle Hawk Owl would be around $500,000. This cost estimate is based off of the bill of materials and labor hours for the manufacture of various components of

the prototype version completed at MIT. The bill of materials includes the engine and supporting equipment, autopilot, servos, PMU, batteries and composite materials. It is assummed that the tooling for manufactured components exists so that the cost to make the tooling is not factored into this estimate. A summarized bill of materials is shown in Table 2.6.

Part	**Quantity**	**Unit Cost**
Composite materials	-	$19,200
DF70 Engine	1	$20,700
Autopilot	1	$12,000
Actuators	8	$140
Avionics Parts	-	$2000
Fuel Tank	2	$2000
Ground Station Equipment	-	$2100

Table 2.6: Bill of materials for JHO.

Chapter 3

Ground Testing Report

Extensive ground testing was completed to evaluate component structural integrity, measure engine performance, and demonstrate system reliability. This section discusses a wing structural test at flight test weights. Engine ground tests are discussed which were completed to measure performance and improve engine reliability. Additionally, system ground tests were done prior to each flight test as a risk reduction measure.

3.1 Wing Structural Test

To verify the structural integrity of the wing before flight, the aerodynamic forces were simulated by hanging discrete weights across the wing span. The deflection at different stations along the wing was measured and the wing was inspected for delamination. The wing was successfully tested at a 100 lbs load in a 2g loading case with a 50% safety margin. This qualified the wings to support a 100 lbs aircraft during flight.

The test was conducted at the MIT Neuman Hanger. The wing was hung upside down at the root by a beam structure. Water jugs filled to discrete weights were hung at specified intervals, according to Table 3.1, along the span to simulate the lifting forces on the wing. Figure 3.1 shows a comparison between the calculated bending moment from the aerodynamic forces and the simulated load from the discrete weights. The maximum error of the discrete weight loading is less than 1%.

Station #	**Span location (ft)**	**Weight (lbs)**
0	0	0
1	1.5	22
2	3	22
3	4.5	20
4	6	20
5	7.5	18
6	9	8
7	10.5	4
8	12	2

Table 3.1: Wing test weights and spanwise location

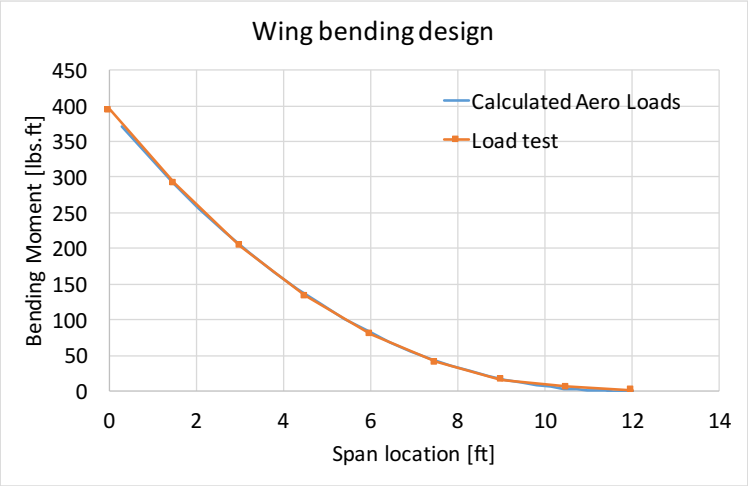

Figure 3.1: Comparison of calculated aerodynamic load vs discrete load test on the wing.

No delamination or fiber breaks were observed after the test. Thus, with the described wing load test the JHO prototype was considered safe to fly up to a 100 lb take off weight. Figure 3.2 shows the wing structural test in its deflected state.

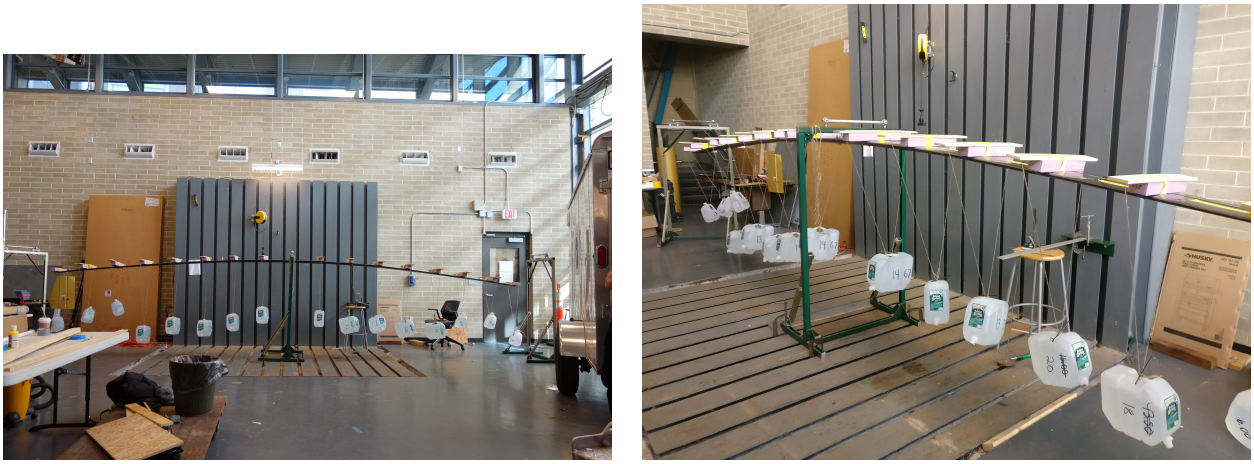

(a) Frontal view

(b) Side view

Figure 3.2: Wing structural test in deflected state.

The ability of the wing to handle the full design load of 150 lbs in a 3g load with a 50% safety margin was in question due to a post-fabrication wing joiner modification. Because it was uncertain if the modification had compromised the integrity of the wing, it was decided that the full design load would not be tested to prevent program delays if the wing failed a load test.

3.2 Engine Testing

Engine ground tests were run for calibration, debugging issues and performance estimates. The DF70 is the primary engine for the JHO. Due to delays in the procurement of the DF70, the TP70 was used for initial flight testing. Ground tests were completed for both engines. Images of the TP70 ground test on a stand and the DF70 ground test on the aircraft on the ground are shown in Figure 3.3.

(a) TP70 ground test on stand

(b) DF70 ground test on aircraft

Figure 3.3: Engine ground test for DF70 and TP70.

3.2.1 Engine Performance Tests

Due to lack of performance data for the TP70 engine, ground tests were completed to evaluate the TP70 performance so that aircraft performance could be estimated if this engine were used. Performance data for the DF70 was taken from the manufacturer. The brake specific fuel consumption (BSFC) was calculated from the fuel flow measured at various engine speeds of the TP70 and compared to DF70 manufacturer data.

This test was conducted by mounting the TP70 on a test stand. A 2 gallon tank holding fuel was connected to the engine and mounted to the back side of the test stand. A third party electronic fuel injection system from Ecotrons was installed to manage fuel burn. The engine was run for 15 min at a constant RPM. The fuel was measured by weight and volume before and after the test. This was repeated for RPM speeds ranging from 4000 to 6000 at 500 intervals. The power generated during the test was estimated from performance data of the 22x8 propeller installed on the engine. The brake specific fuel consumption (BSFC) of the TP70 was estimated by dividing the fuel consumption by the power and test duration. The results were compared to the manufacturer performance data for the DF70 and are shown in Figure 3.4. Both the DF70 data from the manufacturer and the TP70 ground tests completed at MIT were done at static conditions. Based on the ground tests of the TP70, it was concluded that the efficiency of the TP70 was sufficient to achieve the required endurance and was therefore used on initial flight tests.

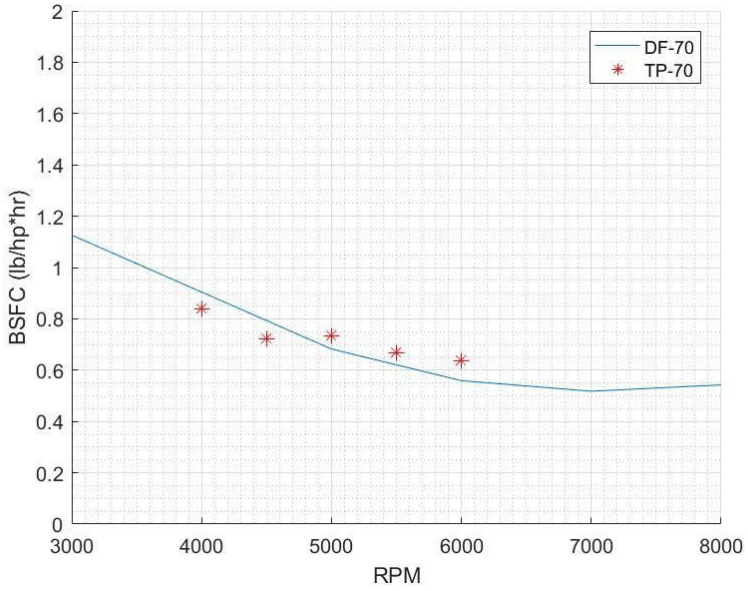

Figure 3.4: Comparison of DF70 performance and TP70 ground test results.

3.2.2 Engine Cooling Ground Test

After the engine cooling had been simulated in SolidWorks, ground and flight tests were required to validate the results. This test was conducted by running the engine on the ground at static conditions while attached to the airframe and covered by the rear fairing. After warming up the engine to 100^oC, the engine was run at maximum throttle for 60 seconds. It was observed that the engine cylinder head temperature rose to about 140^oC and then remained roughly constant. This provides an approximate 20^oC safety margin on engine temperature at a worst case static condition. It was predicted that with additional airflow during flight, a flight test could be conducted with low risk of engine overheating. The in-flight engine cooling test is described in the V1 flight testing section.

3.2.3 Engine Vibration

Both the TP70 and DF70 engines cause significant vibration on the aircraft. This can be a potential hazard if structural components or avionics hardware become loose or disconnected or if servo actuation becomes vibration induced. Vibrational issues were identified by running the engine while installed on the aircraft for 30 min at various RPM settings. Mounting bolts and hardware were checked for tightness following the engine test. Lock nuts andor LockTight were applied as necessary. Avionics components were also checked for loose wires. Connections were replaced or soldered as necessary.

It was observed during a ground vibration test that the throttle servo would jitter or fluctuate for a given input. Consequences for this behavior could include engine shut off during flight, uncontrollable flight behavior, and uncorrelated fuel flow data. After investigation it was determined that the center of mass of throttle body, consisting of the air valve for both cylinders and linkage between the two throttle bodies, was not centered on the air valve causing a throttle pulsing motion proportional to the offset distance. This problem was solved by placing small weights to equal to the weight of the linkage bar on the opposite end of the throttle body, centering the mass of the system. Figure 3.5 shows how the additional weights solve the weight offset issue. Additionally, a ferrule was placed on the throttle servo wire to prevent any signal interference. These changes significantly reduced the throttle fluctuations such that this behavior was not observed in later ground tests or flight tests.

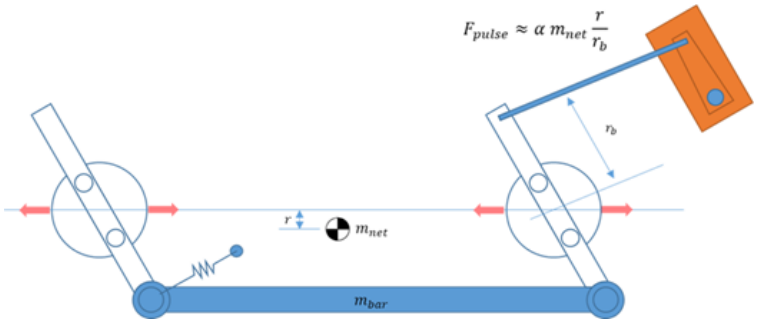

(a) Throttle body configuration with no modifications

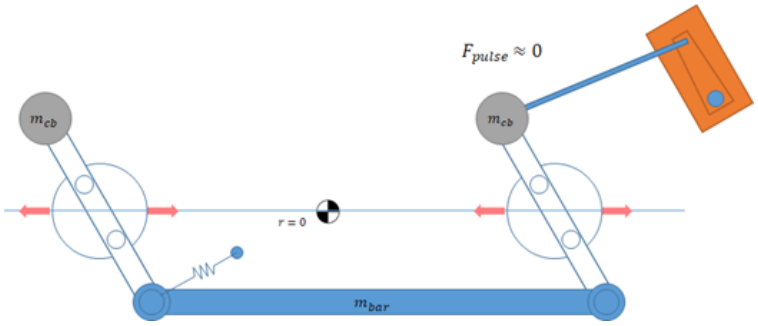

(b) Throttle body configuration with added weights

Figure 3.5: Throttle servo and throttle body diagrams and images.

3.2.4 Engine Reliability

Two issues related to the ECU appeared after multiple ground tests of the DF70: ECU power failure and fluctuating fuel pressure readings. After multiple ground tests of the DF70 it was observed that the vibration of the engine had caused the wire insulation to the ECU power lines to be cut by the ECU chassis. The insulation was replaced with a high durability plastic, solving the issue.

During initial ground tests with the DF70 it was observed that fuel pressure fluctuated between 1.5 and 5 bar as shown in Figure 3.6. It was identified that over time the tubing attached to the pressure sensor inside the ECU expanded under the compression loads of the casing, causing fuel leakage and fluctuating pressure readings. An aluminum sleeve was place around the fuel line inside the ECU to prevent the fuel tubing from expanding and eventually leaking.

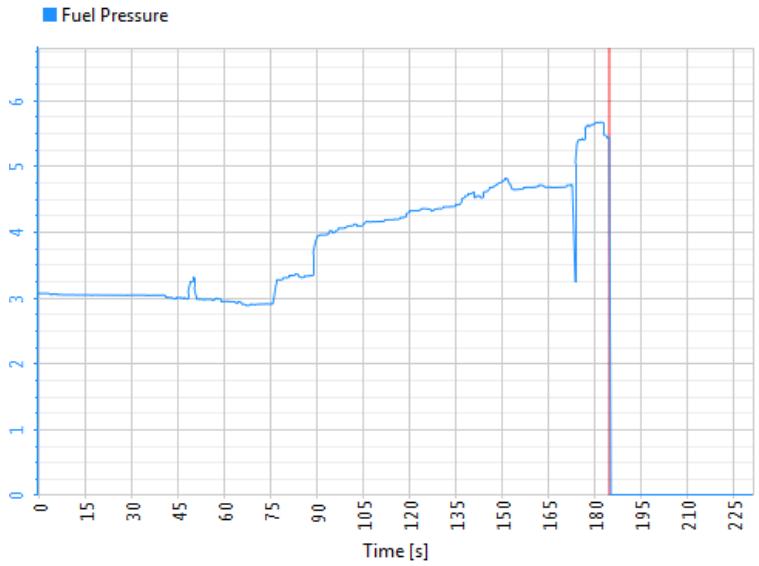

Figure 3.6: Undesirable pressure rise during engine ground test.

There have been no recurrences of these issues after implementing the described solutions. After communicating with RCV Engines, Ltd. it became apparent that because the DF70 is a relatively new engine, there may be additional issues that have not been encountered.

3.3 Range Testing

A manned flight test was conducted which tested the range of all three primary link systems: data radio link for communication with the pilot, RC control link for manual control, and FTS radio link. A general-aviation aircraft carried all 3 systems. Receivers were mounted on the aircraft with a clear line of sight to ground station location. LED lights were connected to the command receivers and were powered on if there was a link with the ground station. The mount for the receivers on the aircraft is shown in Figure 3.8.

The multipath/interference effects of the GA aircraft body are expected to be detrimental to link quality, therefore the test was conservative. This test demonstrated that with the specified receivers and transmitters command links between the receivers and ground station have a link budget beyond 6.5 miles. With the directional receiver for the flight termination system a link budget of 9 miles was demonstrated. A diagram of the test (for one of the primary systems) is shown in Figure 3.7.

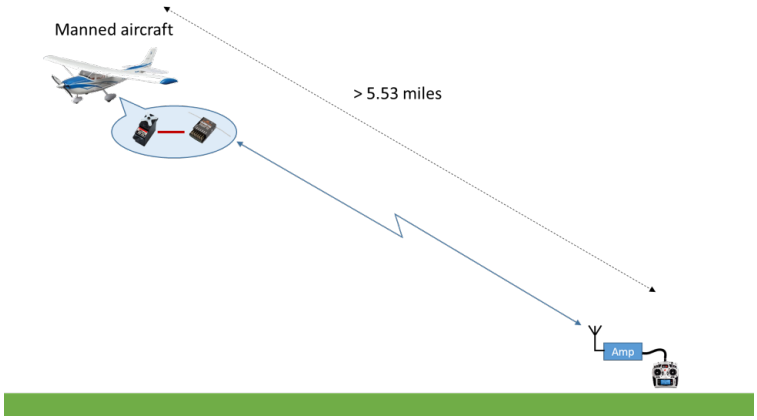

Figure 3.7: Link test in manned aircraft.

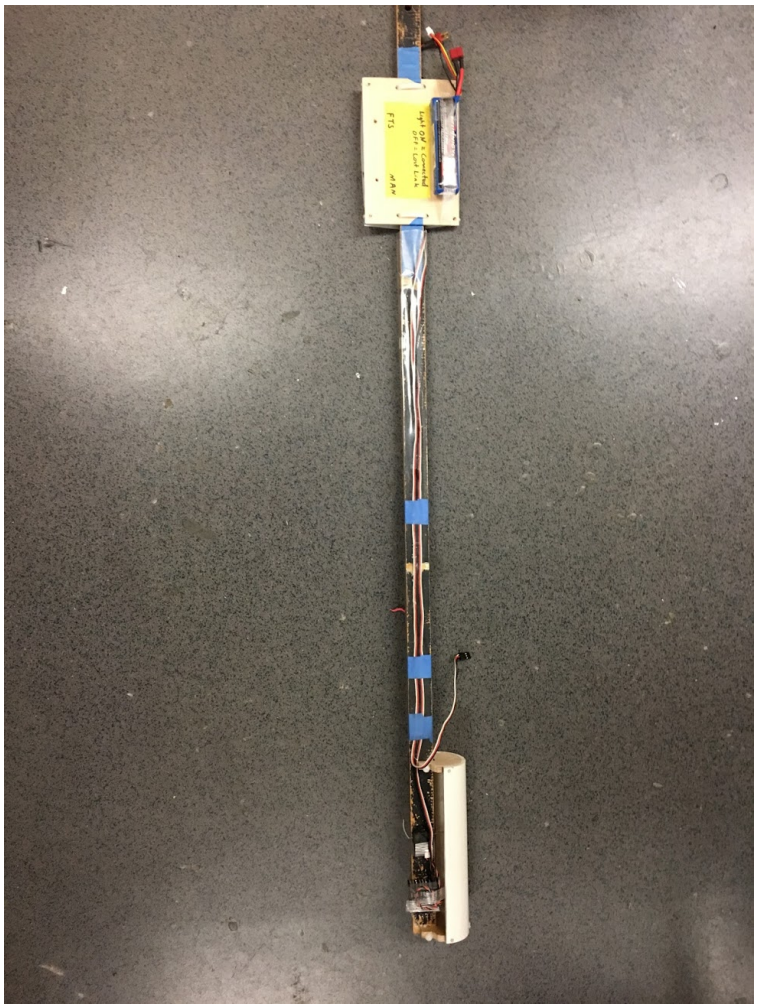

Figure 3.8: Reciever mounting rod for link test.

Figure 3.9 maps the recorded distances where a link was established from the ground station to the aircraft and receivers.

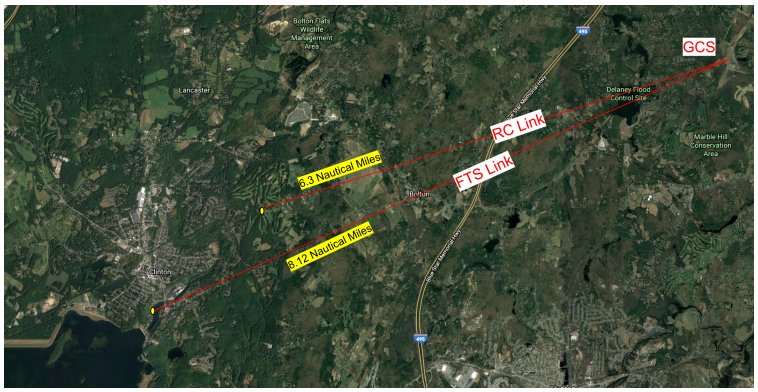

Figure 3.9: Recorded distances with established link between groundstation and receivers.

3.4 Pre-flight Systems Tests

In the days prior to each flight, the aircraft was run through a series of system checks to minimize the risk of an in-flight failure. These system checks included:

- Engine test with acceptable pressure, cylinder head temperatures and vibration
- Control systems checks including ailerons, flaps, elevator, rudder and throttle
- Communications checks of the MicroPilot radio link and RC control link
- Weight and balance checks
- Data logging checks on the MicroPilot and RaspberryPi
- Autopilot settings and waypoint checks
- Safety protocol checks including geofence boundaries and programmed failure mode behavior

These system checks were conducted by assembling the aircraft at MIT and completing the safety checklists.

During the system checks it was identified that about every 1 in 20 instances, the PMU would send a power surge of 8-10V on the 5V line during power up, which would damage the RaspberryPi. Two "keys" are used to power the aircraft from the 24V and 5V lines that output from the PMU. The 24V line is plugged in first, which powers on the engine ECU, Mircopilot, and payload. The 5V line is then plugged in, which powers the RaspberryPi and additional sensors. To power off, the 5V line is disconnected first, then the 24V line. An operational solution was chosen instead of a surge protector to minimize added cost and complexity to the system.

Chapter 4

V0 - Low Weight and Low Altitude Flight Testing

Because the JHO dry weight was under 55 lbs initial flight tests could be done under the FAA Part 107 regulation while certification and approval were pending to test at higher weights and altitudes. The FAA Part 107 regulations restrict flight to under 55 lbs and under 400 ft. Given these restrictions, the objectives of these initial tests were to demonstrate the landing and recovery systems, demonstrate the autopilot systems, determine the aircraft handling qualities and test the avionics system.

4.1 V0 Testing Location

It was decided to do the V0 tests at the Plum Island Airport (2B2). This location was chosen because of its proximity to MIT, low utilization, and unobstructed line of sight surrounding the airport. A map of the Plum Island Airport with a sample autopilot waypoint mission is shown in Figure 4.1.

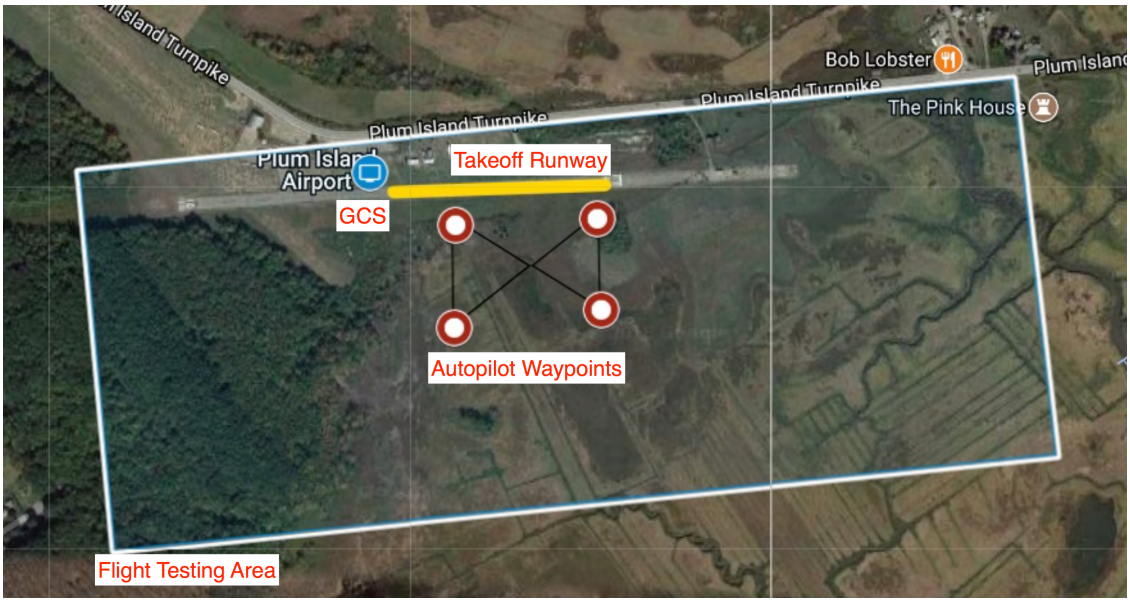

Figure 4.1: Plum Island (2B2) V0 testing location.

4.1.1 V0 Testing Configuration

To reach the 55 lbs required for the Part 107 regulation and carry a few pounds of fuel, a few non-flight-essential items were removed. The JHO was designed with a 10 lb payload in the nose cone. Without this payload the aircraft is unbalanced and rearward components such as the alternator and rear fairing were removed from the aircraft to both reduce the weight and help the balance the center of gravity (CG). Instead of installing the manufactured aluminum fuel tank, a small 2.5 gallon fuel tank was placed in the front of the aircraft to shift the CG forward. Initial flight tests were done with the TP70 while the DF70 was in the procurement process. Figure 4.2 shows the configuration of the aircraft during the V0 tests.

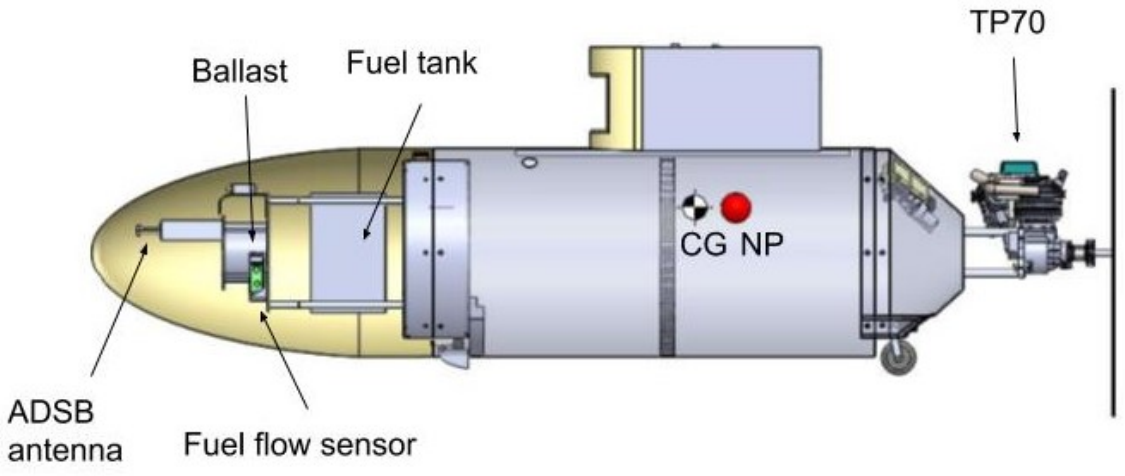

Figure 4.2: V0 test flight configuration.

4.2 V0 Testing Summary

Table 4.1 shows a summary of each flight conducted in this configuration. These tests were conducted at the Plum Island airport. The V0 tests were able to successfully demonstrate the launch and recovery systems and assess the basic aircraft handling qualities. However, significant reliability issues were experienced with the TP70 engine, which are discussed herein. When the TP70 was replaced with the DF70 in later V0 tests, an initial demonstration of the autopilot was achieved. During an 80 minute flight, initial autopilot tuning was completed.

4.2.1 Launch and Recovery

The V0 tests were able to successfully demonstrate the launch and recovery systems. A minor refinement to the launch rack was made following the second flight test during which a combination of bumpy roads and higher wind speeds prematurely knocked the aircraft out of the launch cradle. This caused minor damage to the right wing and fuselage. A positive release solenoid was installed on the launch rack. The solenoid is operated through RC control and holds the aircraft to the launch rack until the operate gives the release command through the transmitter. This component and the launch procedure are described in greater detail in Section 2.6.

Test #	Date	Airport	Winds	Configuration	Description of Flight	Time
1	11-May-17	2B2	9 kts NNE, low cross-winds	Engine: TP70 Launch Vehicle: Mazda 3	JHO first flight. Pilot controlled maneuvering over the field.	10 min
2	22-May-17	2B2	10 kts SSE	Engine: TP70 Launch Vehicle: Mazda 3	Aircraft strike during takeoff.	0 min
3	10-Jun-17	2B2	4 kts WSW	Engine: TP70 Launch Vehicle: Mazda 3	Pilot controlled maneuvering over the field.	15 min
4	10-Jun-17	2B2	4 kts WSW	Engine: TP70 Launch Vehicle: Mazda 3	Maneuvering and PID tuning.	20 min
5	29-Jun-17	2B2	9 kts WSW	Engine: TP70 Launch Vehicle: Mazda 3	Maneuvering and PID tuning.	20 min
6	29-Jun-17	2B2	9 kts WSW	Engine: TP70 Launch Vehicle: Mazda 3	Maneuvering and PID tuning.	55 min
7	29-Jun-17	2B2	9 kts WSW	Engine: TP70 Launch Vehicle: Mazda 3	Maneuvering and PID tuning.	20 min
8	10-Jul-17	2B2	9 kts WSW, 18 kt gusts	Engine: TP70 Launch Vehicle: Mazda 3	Maneuvering and PID tuning.	15 min
9	10-Jul-17	2B2	9 kts WSW, 18 kt gusts	Engine: TP70 Launch Vehicle: Mazda 3	Maneuvering and PID tuning.	25 min
10	14-Aug-17	2B2	9 kts S	Engine: DF70 Launch Vehicle: Mazda 3	Maneuvering and PID tuning.	30 min
11	29-Aug-17	2B2	9 kts ESE	Engine: DF70 Launch Vehicle: Chevy Silverado	Maneuvering and PID tuning.	27 min
12	29-Aug-17	2B2	9 kts ESE	Engine: DF70 Launch Vehicle: Chevy Silverado	Maneuvering and PID tuning.	19 min
13	1-Sep-17	2B2	13 kts WNW, 20 kt gusts	Engine: DF70 Launch Vehicle: Ford Explorer	Maneuvering and PID tuning.	80 min
14	5-Oct-17	2B2	12 kts NE	Engine: DF70 Launch Vehicle: Ram 2500	Maneuvering and PID tuning.	5 min

Table 4.1: Summary of V0 Flight Tests

(a) JHO on launch rack

(b) JHO immediately after take off.

Figure 4.3: Images of the JHO before and after take off.

No significant problems were identified with the recovery operation. The landing gear which consist of a roller blade wheel attached to the rear bulkhead and a stainless steel skid attached to the front bulkhead were adequate for the landing operations even on landings where 2g forces were experienced. Because the propeller radius is larger than the fuselage radius the landing operation is done with the engine powered off. During about 80% of the flights completed during the V0 testing, the propeller stopped horizontally. Because the propeller is frangible, when the propeller did stop vertically it broke off causing no damage to the engine or aircraft. Due to the significant ground effect from the wings, the flap settings were modified to increase the deflection angle, providing increased drag during final approach and landing.

(a) JHO during approach

(b) JHO during landing

Figure 4.4: Images of the JHO before and during landing.

4.2.2 Handling Qualities

The pilot recorded that the overall handling qualities of the JHO were satisfactory during the V0 testing. The aircraft was stable during all stages of flight and responsive to flight control commands. The control surfaces were found to be adequate to maneuver the aircraft at desired rates, trim the aircraft during all stages of flight, and correct for undesired flight behavior.

A few minor deficiences were observed by the pilot during V0 testing. A noticeable phase lag in pitch control (0.2-0.5 second) was experienced. It was hypothesized that this lag was caused by the flexibility of the tail boom in comparison to the pitch inertia of the aircraft forebody. During elevator deflection inputs, the tail boom deflected by a few degrees, which altered the angle of attack of the horizontal tail and delayed its torque transfer to the main body. This lag was addressed for the V1 testing by enlarging the outer diameter of the tail boom from 1" to 1.89", adding extra strength and stiffness.

Flying the vehicle at near-empty weight posed a climb-controllability problem when operating with the TP70 engine. The minimum-operable throttle setting (prior to engine shutoff due to compression loading) generated more thrust than what the aircraft required for cruise. As a result, the aircraft would naturally climb or accelerate. This was temporarily solved by trimming the aircraft with a lowered flaps setting to increase the airframe drag. While the lowered flaps setting increased the liklihood of a wingtip stall behavior, the rudder deflection was found to be sufficient to prevent an adverse-roll due to a stalled wingtip. The climb or acceleration behavior was minimal when operating with the DF70.

4.2.3 Engine Reliability

The DF70 is the primary engine for the JHO. Due to procurement delays, the low cost alternate engine, TP70, was used on initial flight tests. While at a low price point, the TP70 proved to be unreliable. Of the 8 flights completed with the TP70 engine, 6 tests were terminated due to an engine failure.

Later tests in the V0 phase proved the DF70 to be much more reliable. The DF70 only failed on the last test, and the longest flight achieved with the DF70 almost doubled what was achieved with the TP70. For this reason, it is recommended that the TP70 not be used on the JHO and that the DF70 be used or engine of similar quality. The failure on the DF70 occurred due to a detached muffler. The muffler, which also serves as a structural component detached from the cylinder causing the cylinder to also loosen from the crank case. This issue was resolved by returning the DF70 to RCV Engines for servicing and repair.

Chapter 5

V1 - Higher Weight and Altitude Fight Testing

The objectives of the V1 flight testing were to evaluate aerodynamic performance for endurance estimates and demonstration full systems capability.

Figure 5.1: JHO in flight at the Cape Cod Coast Guard Air Station.

5.1 V1 Testing Location

It was decided to operate over the Joint Base Cape Cod because of a restricted airspace region, R4101 over the JBCC that allows UAV flights up to 9000 ft and because of its proximity to MIT. Because the range itself has no runway and operable roads have poor visibility, it was desirable to conduct launch and recovery operations from the neighboring Coast Guard Air Station Cape Cod (KFMH airport). The high level test plan included launch from the Coast Guard Air Station, transit into R4101, system tests in R4101, transit back to the Coast Guard Air Station and recovery from the launch location.

Two geofences were implemented around KFMH airport and the R4101. If the first geofence is breached the autopilot commands the aircraft to return to a rally point inside the R4101. If the second geofence

is breached the on-board computer alerts the ground station so that the FTS can be deployed. Figure 5.2 shows a map of the restricted airspace R4101, the Coast Guard Air Station, aircraft geofences, nominal flight path and ground station.

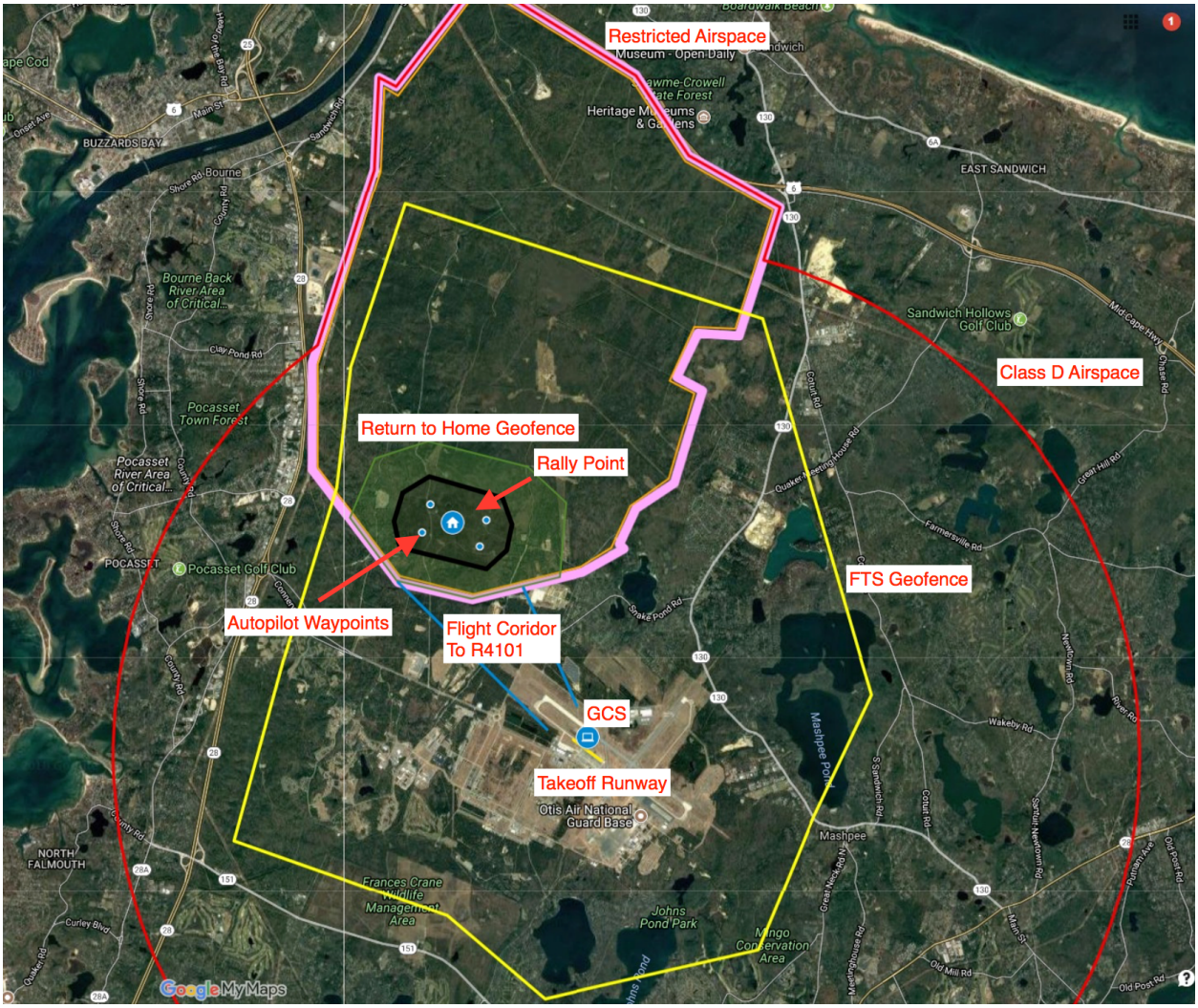

Figure 5.2: Flight testing area at JBCC Coast Guard Air Station and restricted area R4101.

It was determined that initial V1 flight tests would be conducted directly over the Coast Guard Air Station so that autopilot tuning could be completed at higher weights. Figure 5.3 shows the flight testing area during flights completed just over the Coast Guard Air Station.

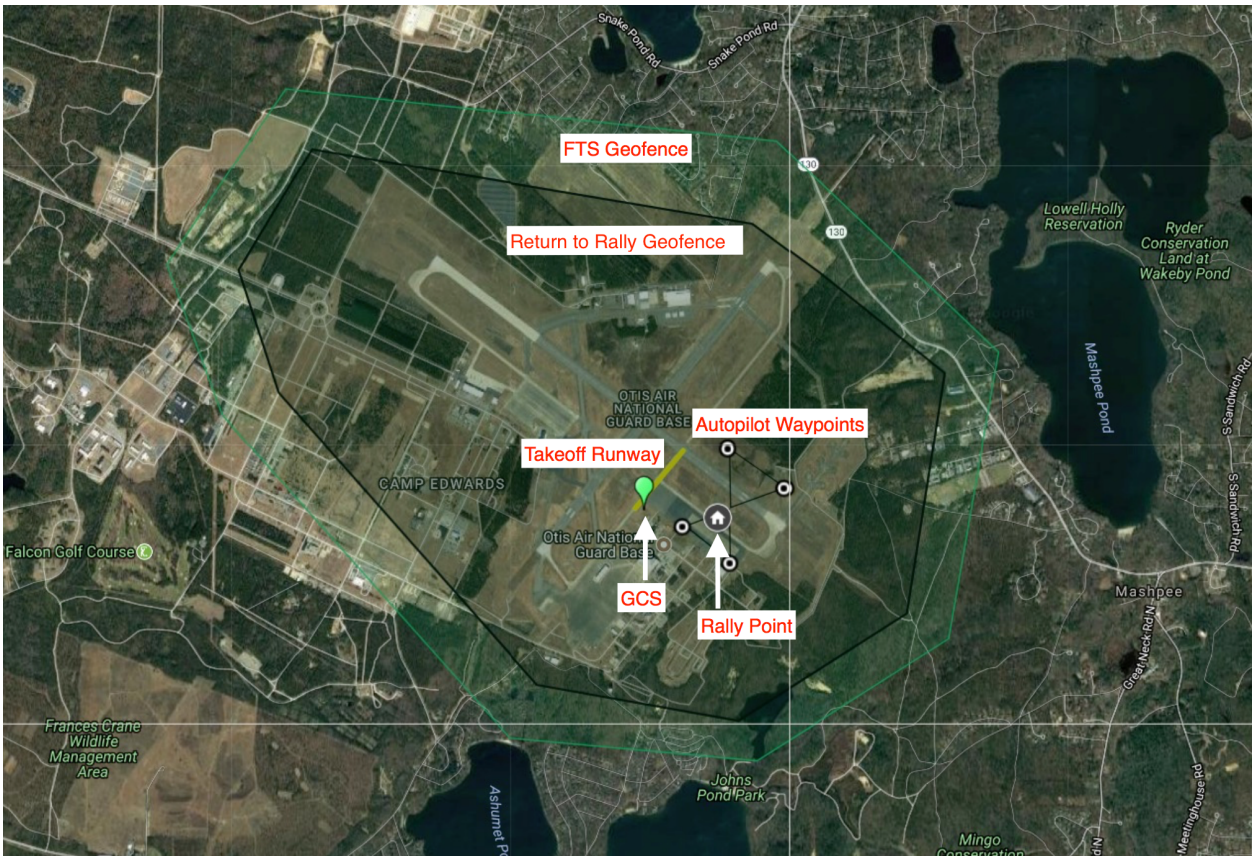

Figure 5.3: Flight testing area over the Coast Guard Air Station.

Approval to fly in the restricted area R4101, is granted by the Army Range Control at JBCC. The Army Range Control required flight test plans, hazard assessments and risk mitigations plans, safety of flight declaration, vehicle descriptions and performance and in person meetings before approval was given to operate over the JBCC.

In order to launch and recover from the Coast Guard Air Station Cape Cod a certificate of authorization (COA) from the FAA was required because the airspace over the Air Station is classified as class D airspace. The COA from the FAA was applied for and received through an organization called Nuair that operates out of Griffiths Air Base in New York but has ties to the Massachusetts Department of Transportation program for UAV testing and development. The application for the COA also required vehicle characteristics and performance, risk assessment and protocols, communications frequencies and airworthiness assessment provided by Nuair. Because the Nuair applied for and received the COA, MIT leased the JHO to Nuair and conducted all their operations under Nuair jurisdiction.

Finally, approval was also needed from the Coast Guard to operate out of the Air Station. This approval was obtained by submitting the COA, lease agreement between MIT and Nuair, and risk and safety documents and by signing a letter of agreement with the Coast Guard regarding operating procedures. All supporting documents for the Army Range Control approval, COA, and Coast Guard approval are attached to this document.

It is noted here that airworthiness approval through the Air Force was investigated and initiated. Ultimately, because this was not directly needed to operate at the JBCC, this option was not pursued.

5.2 V1 Testing Configuration

To demonstration the full system during V1 flight testing, components that had been removed for the V0 were reinstalled on the aircraft including the rear fairing, alternator, and aluminum fuel tank. A fuel flow sensor was also installed to measure the aircraft performance. Figure 5.4 shows the aircraft configuration for the V1 flight tests.

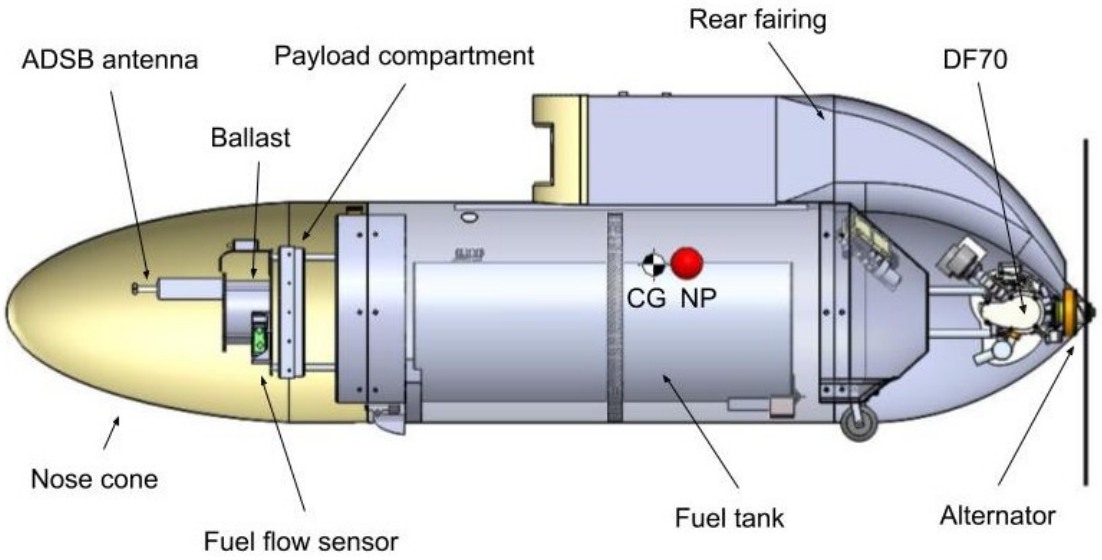

Figure 5.4: JHO configuration for V1 testing.

5.2.1 V1 Fuel Tank

For the V1 testing an aluminum fuel tank was designed and manufactured at MIT. The total capacity is 9 gallons and weighs of 8.2 lbs. The fuel tank design and manufactured part is shown in Figure 5.5. A fueling port is located on the top surface of the tank and is accessible from the side of the fuselage. Baffles throughout the tank prevent sloshing. The sump at the rear of the fuel tank ensures fuel draw during aircraft maneuvers. The custom design fuel tank capable of holding 15 gallons from AeroTec was not manufactured or used during flight testing due to time and cost constraints.

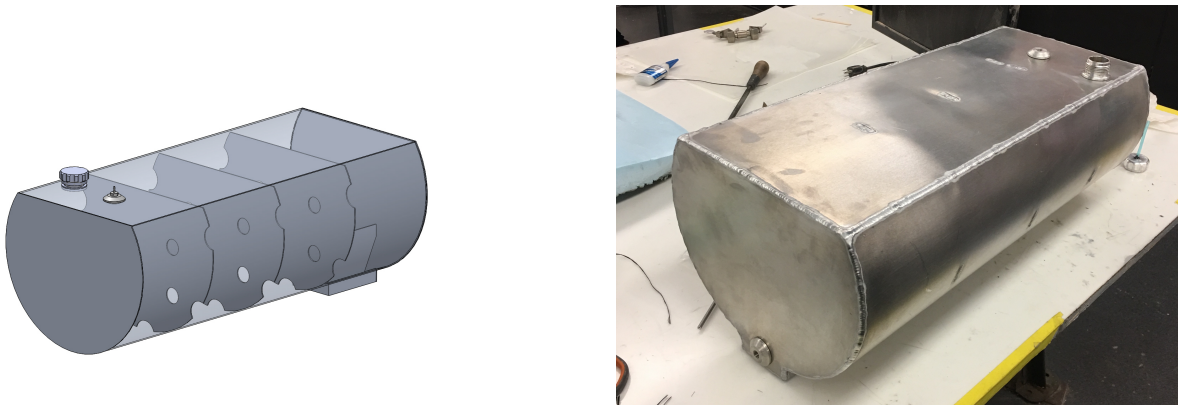

(a) Fuel tank design

(b) Manufactured fuel tank

Figure 5.5: Fuel tank design and manufactured part.

5.2.2 Engine Modifications

To enable V1 testing, the alternator was installed on the engine and the 3 phase AC cables were connected to the PMU to power the aircraft. The ECU electrical system was also modified to allow parameters to be read by the RaspberryPi and transmitted to the MircoPilot. This enabled live engine telemetry updates on the ground control station.

5.2.3 Fuel Flow Installation and Calibration

The Sensirion Flow Meter SLI-2000 was installed on the aircraft to measure fuel flow for V1 testing. The JHO is estimated to burn about 8 mL/min. The Sensirion is one of a few flow sensors capable of measure flow rates that slowly and is rated for fuel. The Sensirion uses temperature gradients and resistance to measure the fuel flow rate. The fuel flow sensor was mounted on vibrathane at the front of the aircraft to minimize vibration and get more accurate readings. An image of the Sensirion installed on the aircraft is shown in Figure 5.6.

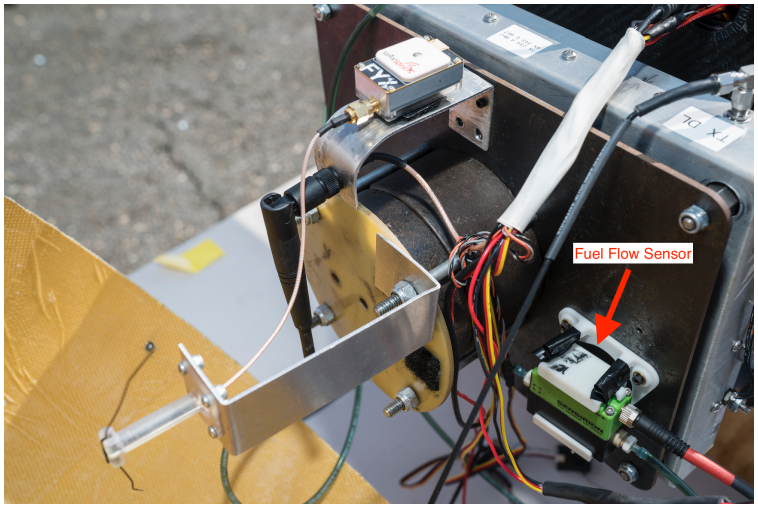

Figure 5.6: Image of installed fuel flow sensor in the front of the JHO.

Because the Sensirion is calibrated for water, additional testing had to be done to calibrate the measurements for gasoline. Various known quantities of fuel were drained through a pipette with the fuel flow sensor

in line. The integrated fuel flow measurement taken by Sensirion was compared to the actual fuel used. The correlation between the known and measured fuel quantities was used to calibrate the Sensirion to gasoline.

There still remains some uncertainty regarding the fuel flow measurements taken during flight because of the engine induced vibration.

5.3 V1 Testing Summary

Table 5.1 shows a summary of the V1 flight tests. During the V1 testing, the full system capability was demonstrated and fuel flow measurements were taken to evaluate endurance performance. The performance evaluation is discussed in Chapter 6. The payload was demonstrated during the final 3 flights and is discussed in Chapter 7. While full autonomous flight was demonstrated for short periods of time, abnormal behavior from the autopilot was observed multiple times during the V1 testing. For this reason, it was decided to restrict flight to visual line of sight only for easy RC recovery. Because entering the restricted airspace R4101, would have been a BLOS operation it was not attempted during the V1 testing.

Test #	Date	Airport	Winds	Configuration	Description of Flight	Time
15	9-May-18	KFMH	4-8 kts NE	Engine: DF70 Launch Vehicle: Ford F250	Nominal takeoff and RC control. Attempted autopilot PID tuning.	31 min
16	25-May-18	KFMH	7 kts SW	Engine: DF70 Launch Vehicle: Ford F250	Attempted autopilot PID tuning.	69 min
17	12-Jun-18	KFMH	15 kts NNE	Engine: DF70 Launch Vehicle: Ford F250	Instrumentation error 5 min into flight.	5.5 min
18	12-Jun-18	KFMH	15 kts NNE	Engine: DF70 Launch Vehicle: Ford F250	Attempted autopilot PID tuning. Completed glide tests.	47 min
19	22-Jun-18	KFMH	15 kts, 20 kt gusts NNE	Engine: DF70 Launch Vehicle: Ford F250	Attempted autopilot PID tuning. Completed glide tests.	45 min
20	22-Jun-18	KFMH	15 kts, 20 kt gusts NNE	Engine: DF70 Launch Vehicle: Ford F250	30 minutes autonomous flight.	47 min
21	20-Jul-18	KFMH	11 kts SE	Engine: DF70 Launch Vehicle: Ford F250	Lincoln Labs payload demonstration	75 min
22	20-Jul-18	KFMH	11 kts SE	Engine: DF70 Launch Vehicle: Ford F250	Manual controlled flight for fuel measurements.	45 min
23	6-Aug-18	KFMH	11 kts SE	Engine: DF70 Launch Vehicle: Ford Explorer	Payload demonstration. Loss of control, flight terminated.	55 min

Table 5.1: Summary of V1 test flights.

5.3.1 V1 Handling Qualities

The pilot observed the handling qualities of the JHO to also be satisfactory during the V1 testing. In terms of the airframe dynamics for normal flight, the pilot noted that the V1 configuration performed well. Motion along all axes (roll, pitch, yaw) are responsive and well-damped.

In the V1 aircraft, the pitch-lag problem was mitigated by increasing the tail boom diameter from 1" to 1.89". This change greatly increased the bending stiffness of the tail boom and greatly reduced the pitch response lag.

In addition, the larger fuselage mass and switch to the DF-70 engine with smoother dynamics and lower-operable-thrust improved climb-controllability. At the minimum-operable throttle, the aircraft was able to descend slowly. To aid in climb-rate control, a throttle-curve map was programmed into the transmitter to allow the lower 50% of the transmitter's throttle stick travel to control the lower 20% of the throttle valve travel, giving sufficient control resolution to allow the pilot to zero out the aircraft's climb-rate using throttle.

While the landing operation was completed successfully for each flight, the pilot obeserved that landing at lower vertical speeds to minimize the shock absorption by the landing gear was challenging due to a combination of effects. Firstly, because the engine is off during landing, the lack of propeller rotation removes the wake-filling effect increasing the fuselage drag's sensitivity to angle of attack. Therefore, high angles of attack reduce aircraft kinetic energy more than in other phases of flight. Secondly, the pitch sensitivity of the aircraft is increased due to ground effect on the wing. The combination of these two factors means it is very easy to overcorrect a pitch error while also robbing the aircraft of forward speed, which cannot be replenished due to the necessity of shutting down the engine for landing.

A complicating factor to this handling issue is that of flaps, which are necessary to steepen the glide slope to enable accurate positioning of the aircraft for landing. However, the aircraft's short-span flaps also reduce the maximum lift coefficient of the wing and increase its drag at high Cl.

Through fine tuuning, the pilot developed a reliable method for landing and after engine shut off:

1. Set elevator control rates to low (30% of maximum travel)
2. Lower flaps to steepen glide slope, bleed off energy until aircraft is approximately 15 feet above the runway
3. Raise flaps to increase available Cl and to remove the flap's drag effects at high Cl
4. Wait while the aircraft settles by approximately 5 feet and accelerates due to the raising of the flaps
5. Gently control vehicle in pitch, while keeping in mind that the aircraft will behave as if the control rates were in high mode
6. Expect the flare-glide to run long due to ground effect

This problem may be addressed by redesigning the landing gear to improve its absorption capability.

5.3.2 Autopilot Reliability

The MicroPilot was chosen as an off-the-shelf risk reduction autopilot. However, during test flights 15, 16, 18, 19, and 22 the autopilot commanded the aircraft into a steep dive or a stall position multiple times per flight. The backup RC pilot took control during these moments to stop the undesired behavior. Additionally, during flight test 21 the autopilot entered a "non-recoverable" failure when there appeared to be no failure. The autopilot command for this failure is an autonomous landing. The backup RC pilot also took control during this situation to prevent an unplanned landing.

Multiple unsuccessful attempts were made to improve the reliability of the MicroPilot and prevent the described behavior. This behavior is attributed in part to the non-conventional way in which the autopilot was programmed. Non-conventional logic and extra features deviated from common autopilot practices and likely caused undesired flight behavior. Additionally, hard coded logic and failure modes that cannot be viewed, edited or disabled by the user because it is propriety software may have also caused the undesired behavior.

Finally, the loss of control and terminated flight in flight 23 were ultimately attributed to a MircoPilot PCB board failure which is discussed in Section 5.3.4

5.3.3 Engine Reliability

The DF70 operated reliably for the V1 test flights with no engine failures occurred. A small refinement was made to secure the muffler to the cylinder after flight 15. After this flight it was observed that two of the four bolts attaching the muffler to the cylinder head vibrated loose as shown in Figure 5.7(a). It was decided to secure the four bolts to the muffler using safety wire as shown in Figure 5.7(b).

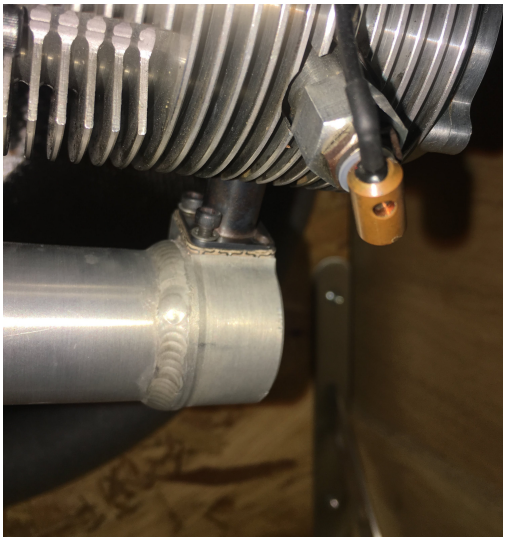

(a) Loose muffler bolts after flight test

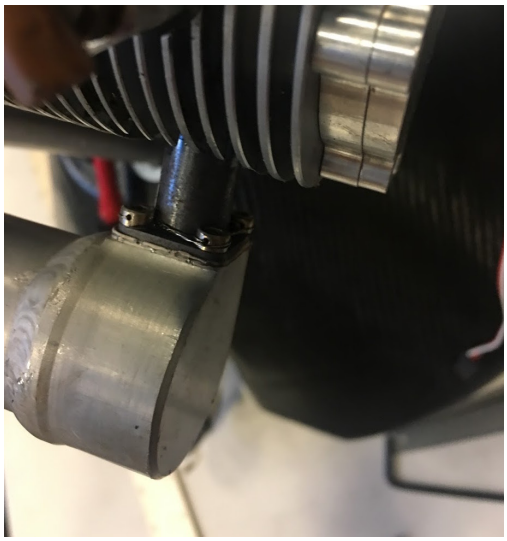

(b) Safety wire on muffler bolts

Figure 5.7: Muffler bolt issue and resolution.

5.3.4 Flight Termination

During the last flight test, the safety pilot noticed that the vehicle had started to deviate from the standard orbit and took over manual RC control. The vehicle did not respond to RC or ground station control commands. It was later determined that the root cause of this loss of control failure was a failed capacitor on the MicroPilot PCB board. This caused a power failure to the autopilot and servos because the servo control and power was routed through the MicroPilot. The damaged component is shown in Figure 5.8. The failed MicroPilot further confirmed our assessment of its unreliability.

The tower was immediately informed of the situation, and when control could not be established, the flight was terminated over the airport boundary and the vehicle entered a descending spiral.

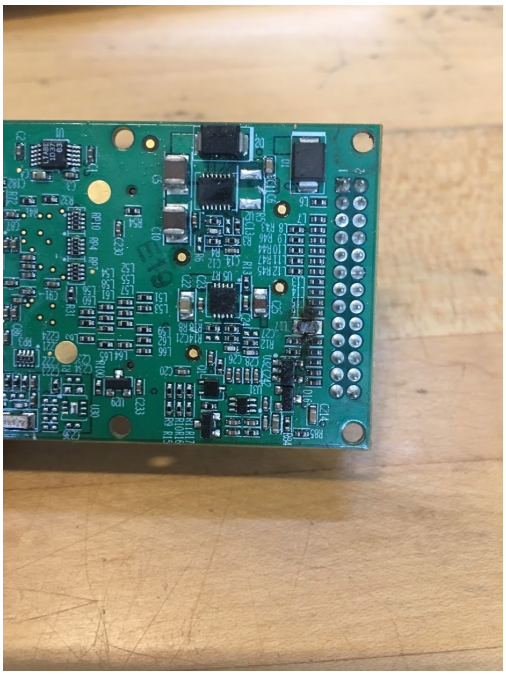

(a) Blown capacitor on MicroPilot

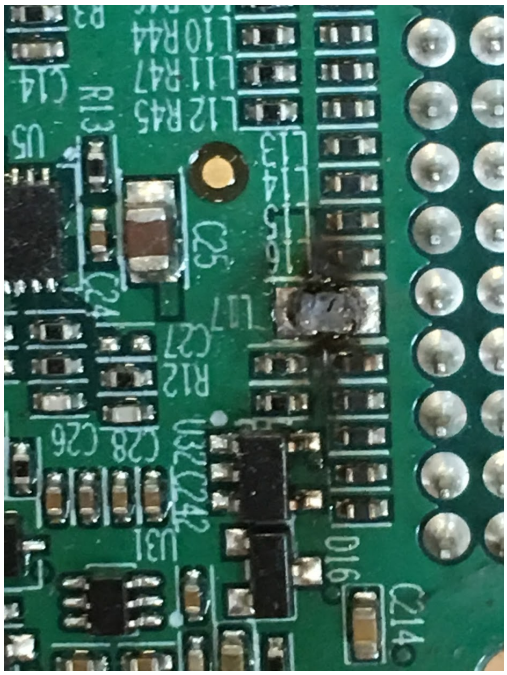

(b) Zoomed in view of blown capacitor

Figure 5.8: Damaged MicroPilot PCB board.

The damaged vehicle was recovered North and West of the airport (Figure 5.9). The official report sent to the FAA and Coast Guard is included in the attachments.

Figure 5.9: Vehicle after flight termination.

Chapter 6

Vehicle Performance

Due to the unreliability of the autopilot and cost and complexity of a multi-day test, the full endurance capability of the JHO was not tested. Instead the endurance was estimated by extrapolating the aircraft performance data. The key parameter used to extrapolate endurance is weight specific fuel consumption ($WSFC$). This is directly measured as

$$WSFC = \frac{\dot{m}_{\text{fuel}}}{W} \tag{6.1}$$

Where $\dot{m}_{\text{fuel}}$ is the fuel flow rate and W is the aircraft weight during that flight segment. From the flight tests, the fuel flow rate is directly measured and the aircraft weight is 85 lbs for the flight tests considered. An example of the fuel flow rate and integrated fuel burn is shown in Figure 6.1.

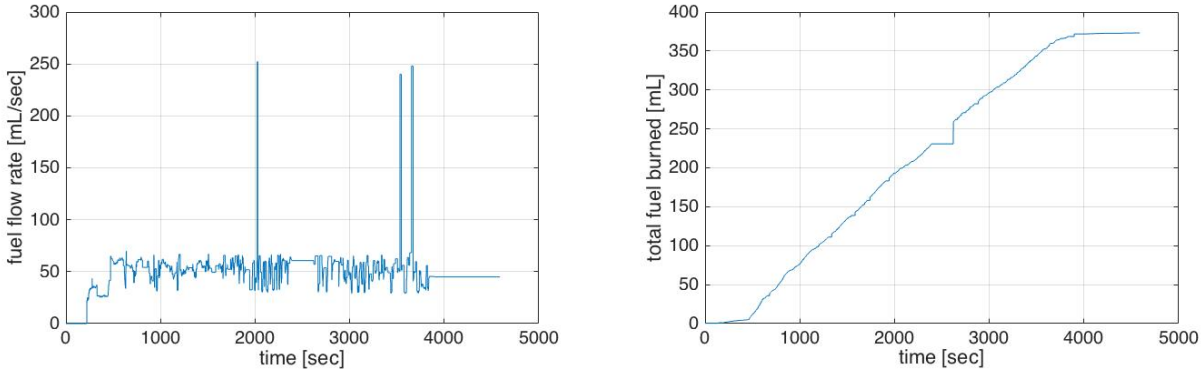

(a) Fuel flow rate

(b) Total fuel burned

Figure 6.1: Fuel burn and fuel burn rate for flight 20.

The $WSFC$ is calculated during portions of relatively level, steady flight by integrating the fuel flow measurement for a given time period on the order of 3-5 min and dividing by the time elapsed. The resulting $WSFC$ are plotted against the corresponding average speed during that time period. The values are shown in Figure 6.2. A parabolic curve is fitted to the data to derive a relationship between flight speed and $WSFC$.

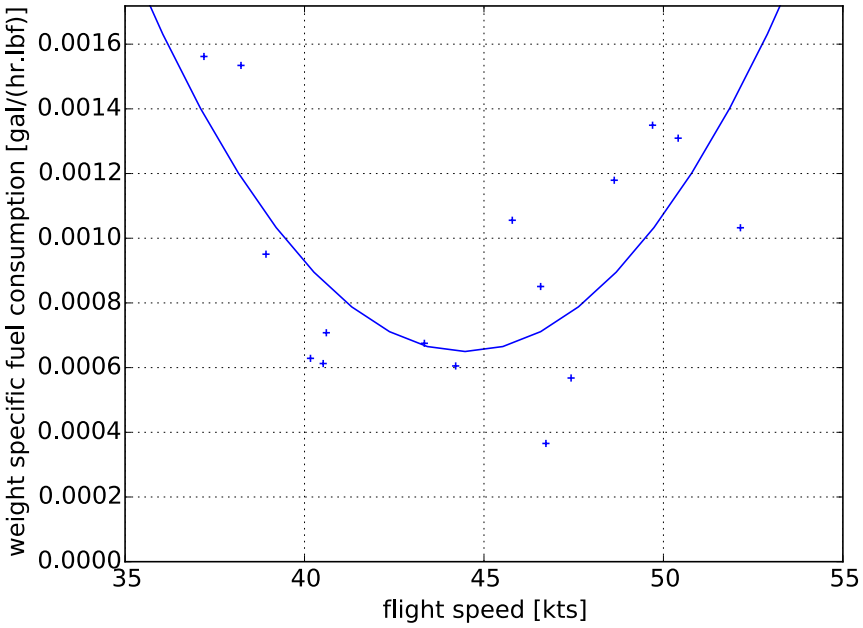

Figure 6.2: $WSFC$ **vs. flight velocity data and fitted function.**

It is noted here that there is likely significant boundary layer injestion from the fuselage that improves engine perofrmance. The effect is captured in the $WSFC$ value, but not explicitly quantified. Future work could include quantification of the increased performance of the boundary layer injestion through wind tunnel testing.

The endurance is calculated using a time marching Breguet range algorithm. At its fullest weight the aircraft will fly faster and will slow down as weight is burned off. If a constant coefficient of lift is assumed, then the value of $WSFC$ will change during flight, starting high at a high velocity, decreasing as velocity decreases and increasing again after the minimum $WSFC$ speed is reached. Figure 6.3 shows how the speed and weight of the aircraft might change during a flight according to the flight data.

Figure 6.3 also shows the optimization results from GPkit for comparision. It is noted that the slope of the speed and weight curves according to the flight test data differs from the optimization results. This discrepency is due to the simplifying assumptions that $WSFC$ and speed have a parabolic correlation and that the coefficient of lift is constant. However, both the flight test data and the optimization results show approximately the same speed and weight change during the flight.

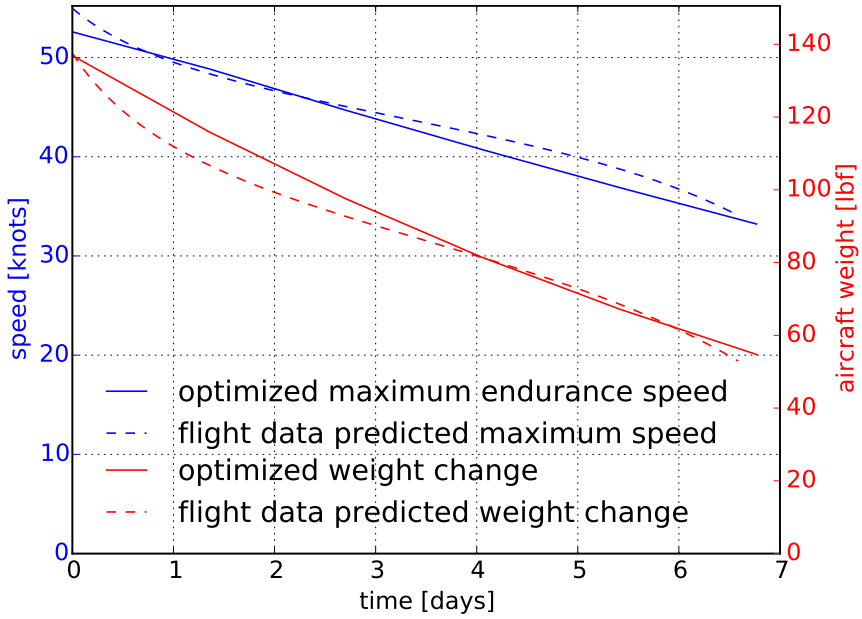

Figure 6.3: Speed and weight change during maximum endurance mission. Dotted curves show the flight test data results. Smooth curves show the GPkit optimized results.

Using the described methodology and flight test data, the endurance of the JHO can be extrapolated to be 6.6 days. This is result is plotted against the optimized GPkit aircraft performance in Figure 6.4. Also plotted in Figure 6.4 is the predicted flight endurance based on the flight test data if you constrain the aircraft to fly at a constant speed for the duration of the mission. This is plotted against the predicted endurance in the GPkit optimization model for the same speed constraint.

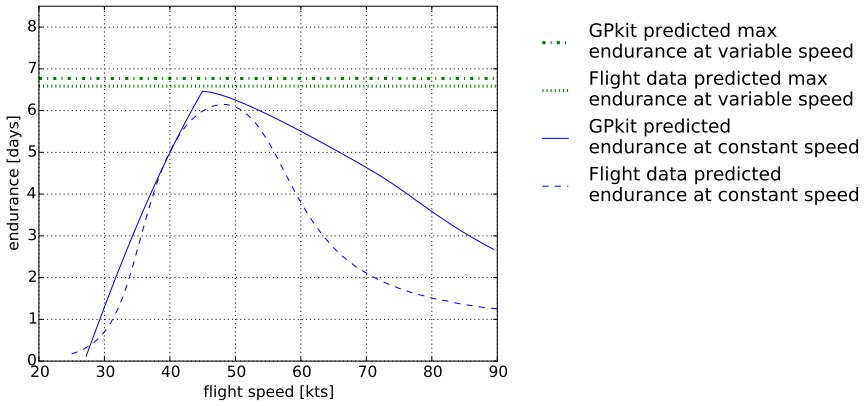

Figure 6.4: Maximum endurance at constant and variable speed as predicted by the GPkit optimization model and flight test results. Dotted curves show flight test data results. Smooth curves show GPkit optimization results.

The slope of the flight data predicted endurance and optimization predicted endurance curves is different again because of the simplifying assumption that $WSFC$ and speed have a parabolic correlation. However, both optimization results and the flight test data agree to within 5% on the maximum endurance achievable and the optimum endurance speed. Thus the flight test data supports the optimization results that the JHO could satisfy the 6 day endurance requirement.

6.1 Engine Cooling Validation

During the flight tests, engine cylinder head temperature was also measured to verify that the engine did not overheat during flight. Figure 6.5 shows that the engine cylinder head temperatures never exceeded 140^{o}C even during an exteded climb portion of flight 18. This demonstrates that the cooling duct and cooling exhaust vent were sufficient to keep the engine temperature below the recommended safety limit of 160^{o}C. Increased aerodyanmic performance may be possible by ducting the cooling around around the cylinder heads.

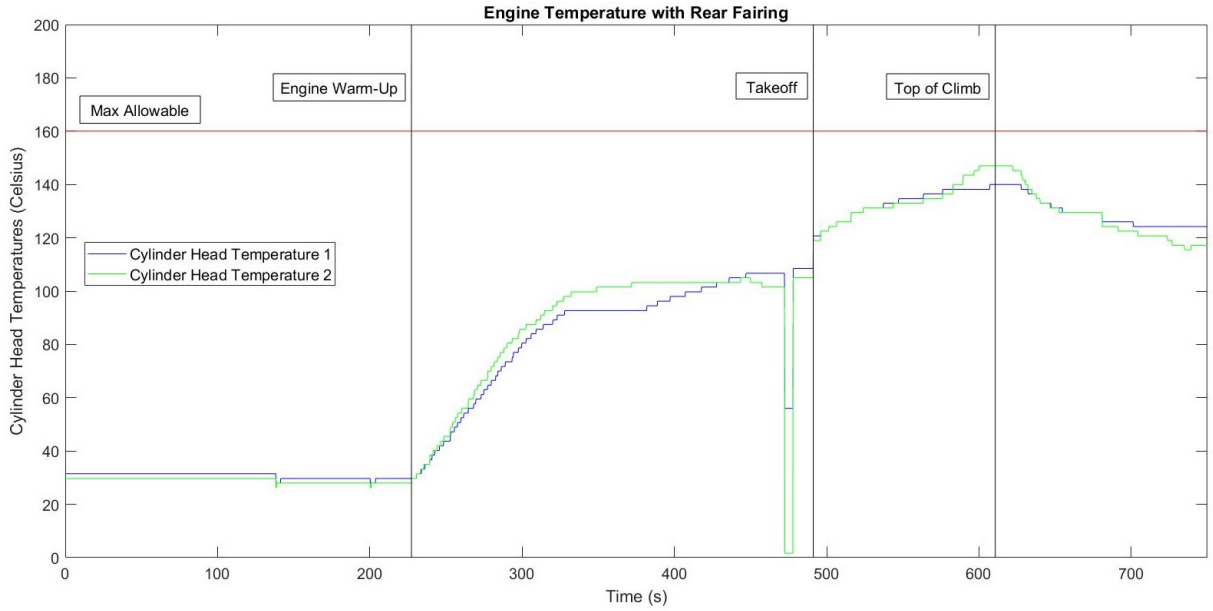

Figure 6.5: Engine Temperature during flight with Rear Fairing

Chapter 7

System Demonstration

The full aircraft and communications system was demonstrated by simulating a communications mission. To accomplish this the Lincoln Laboratory payload was installed on the aircraft. The payload, which is powered by the alternator was successfully tested in air during 3 test flights. The payload functioned as expected for the duration of each flight test. Given the success of these tests and endurance predicted in Chapter **??**, there is a high likelihood that the designed Jungle Hawk Owl vehicle would meet the mission requirements.

The payload comparent was designed for volume and modulatity. The large volume and simple mounting scheme allowed for multiple payload configurations to be mounted and tested. To flight tested payload was installed inside a RF protetive sheild shown in Figure 7.1(b). The shield protected the signals going to and from the payload from the nearby 2.4 GHz autopilot link and ADS link. The shield also doubled as heat sink for the payload. The shield and payload were mounted to the avionics bay lid as shown in Figure 7.1(a). A transmission and reciving antennas were also placed on the aircraft, in the nose cose and on the vertical tail respectively. Figure 7.2 shows the mounted antennas.

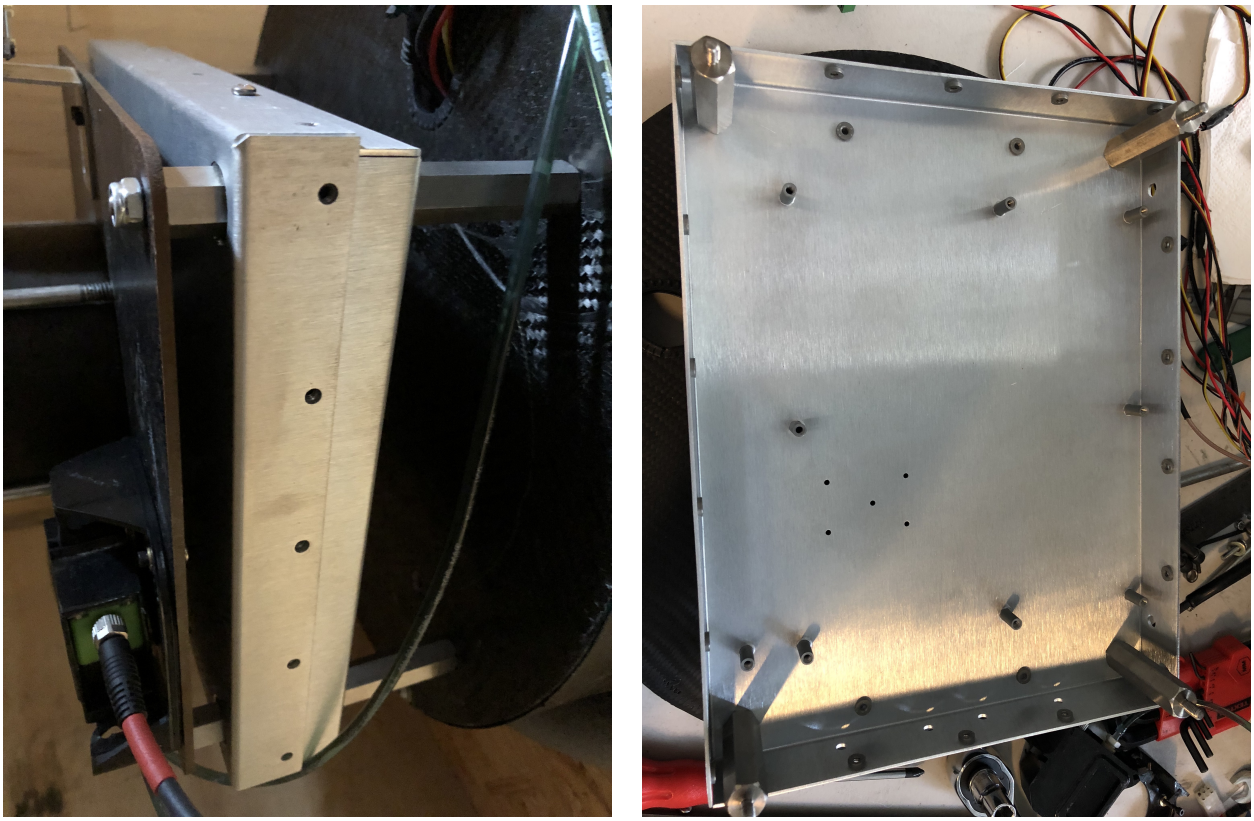

(a) Installed payload and shield

(b) Inside payload shield

Figure 7.1: Payload installation on the JHO.

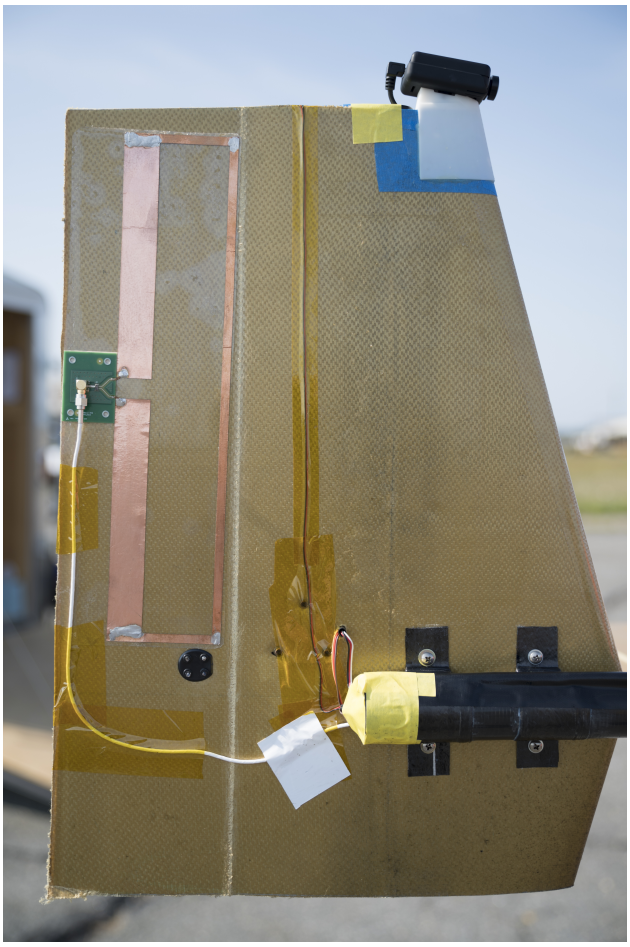

Figure 7.2: Intalled vertical tail transmitting payload antenna.

The payload was operated on flight 21, 22 and 23 and enabled radio communication through the payload. The payload link was demonstrated upto 30 miles away from the ground control station at a flight alitude of 1200 ft. By extrapolation, it is expected that at the design flight altitude of 15,000 ft the coverage would more than satisfy the 100 km diameter footprint requirement.

Chapter 8

Lessons Learned and Recommendations

Based on the flight test results and system demonstration, the MIT team believes the Jungle Hawk Owl design capable of completing a 5 day endurance communications mission. From the flight tests and performance data it can be concluded that the aerodyanmic performance is likely as good as the performance predicted by the GPkit model and that achieving up to 6 days of endurance is possible. Additionally, system demonstration with the customer payload, shows that the intended design communications mission is likely achievable with this platform.

It is likely that aerodyanmic performance could be improved by higher quality manufacturing and improved engine cooling ducting. It is also recommended that the engine performance benefit due to boundary layer ingestion be quantified through wind tunnel testing.

While the aerodyanmic performance appers to be adquate for the mission requirements, it is recommended that a few reliability issues be addressed. The DF70, appears to be a high performing engine according to the performance data. However, because it is a relatively new engine, reliability issues were encountered with the supporting components (ECU, pressure regulator, throttle body). While many issues were addressed during ground and flight testing it is possible that other issues may arise or that implemented solutions may not be adequate when operating continuously for extended periods of time. It is recommended that additional ground testing of the DF70 be completed to verify its reliability.

The TP70 did enable initial flight testing to be accomplished. However, it is recommended that the TP70 not be used with the JHO. Ground and flight tests showed it to be unreliable as it frequently failed during test flights. Additionally, significant modification had to be done on the engine to enable use with an alterator and EFI system. It is possible that other engines of similiar performance performance to the DF70 and TP70 exist and it is recommended that these be researched in greater detail.

The off-the-shelf MicroPilot, initially chosen to reduce risk, also proved to be unreliable. The lack of transparency in the flight control architecture of this autopilot made it difficult to diagnose the observed flight control anomalies. The RC backup pilot frequently had to take control when these anomalies occured. BLOS and high altitude operations could not be completed during the V1 testing as originally planned due to the unreliability of this component. Additionally, the root cause of the flight termination during flight 23 was due to a failure on the MicroPilot PCB board. If possible, it is recommended that an open source or custom built autopilot be used.

To minimize cost and complexity, off the shelf avionics components were selected. Connections between these components on occasion vibrated loose during ground and pre-flight tests despite upgraded connectors and wiring. It is recommended that the electrical bus for the aircraft be upgraded such that vibration induced failures are minimized.